

1 **Title: The genetic architecture of human cerebellar morphology supports a key role for the**
2 **cerebellum in human evolution and psychopathology**

3
4 **Short title: Genetic architecture of cerebellar morphology**

5
6 **Authors:** Torgeir Moberget^{*1,2}, Dennis van der Meert^{†1,3}, Shahram Bahrami^{†1}, Daniel Roelfs¹,
7 Oleksandr Frei¹, Tobias Kaufmann^{1,4}, Sara Fernandez-Cabello¹, Milin Kim¹, Thomas Wolfers^{1,4},
8 Joern Diedrichsen⁵, Olav B. Smeland¹, Alexey Shadrin¹, Anders Dale⁶, Ole A. Andreassen¹ & Lars
9 T. Westlye^{1,7}.

10
11 *Corresponding author

12 †These two authors contributed equally

13
14 **Affiliations:**

15 1: Norwegian Centre for Mental Disorders Research (NORMENT), Division of Mental Health and
16 Addiction, Oslo University Hospital & Institute of Clinical Medicine, University of Oslo, Oslo,
17 Norway

18 2: Department of Behavioral Science, School of Health Sciences, Oslo Metropolitan University -
19 OsloMet, Oslo, Norway.

20 3: School of Mental Health and Neuroscience, Faculty of Health, Medicine and Life Sciences,
21 Maastricht University, The Netherlands

22 4: Department of Psychiatry and Psychotherapy, Tübingen Center for Mental Health, University of
23 Tübingen, Germany

24 5: Brain and Mind Institute, University of Western Ontario, London, Canada

25 6: Center for Multimodal Imaging and Genetics, University of California at San Diego, La Jolla, CA,
26 USA

27 7: Department of Psychology, Faculty of Social Sciences, University of Oslo, Norway

28

29

30

31

32

33

34

35

36

37

NOTE: This preprint reports new research that has not been certified by peer review and should not be used to guide clinical practice.

38 **Abstract current: 154 (limit: 160)**

39 The functional domain of the cerebellum has expanded beyond motor control to also include
40 cognitive and affective functions. In line with this notion, cerebellar volume has increased over recent
41 primate evolution, and cerebellar alterations have been linked to heritable mental disorders. To map
42 the genetic architecture of human cerebellar morphology, we here studied a large imaging genetics
43 sample from the UK Biobank (n discovery = 27,302; n replication: 11,264) with state-of-the art
44 neuroimaging and biostatistics tools. Multivariate GWAS (MOSTest) on empirically derived regional
45 cerebellar MRI features yielded 351 significant genetic loci (228 novel, 94% replicated). Candidate
46 SNPs showed significant positive enrichment for relatively recent genetic mutations over the last
47 300k years (i.e., coinciding with the emergence of Homo sapiens), while gene level analyses
48 revealed enrichment for genes associated with human-specific evolution over the last ~6-8 million
49 years. Finally, we observed genetic overlap with major mental disorders, reinforcing the notion of
50 cerebellar involvement in psychopathology.

51

52 **Teaser:** Genome-wide analysis of cerebellar morphology reveals links to recent human evolution
53 and psychopathology

54

55

56

57

58

59

60

61

62

63

64

65

66

67

68

69

70

71

72

73

74 Introduction

75 The cerebellum contains ~80% of all neurons in the human brain(1) and has rapidly expanded in
76 volume over recent primate evolution(2). Indeed, the surface area of the cerebellar cortex extends
77 to almost 80% of the surface area of the cerebral cortex(3). Comparative genetic analyses suggest
78 that protein coding genes with known roles in cerebellar development have been subject to a similar,
79 or even greater, rate of hominid evolution as compared to cerebro-cortical developmental genes(4).
80 Thus, the evolution of the cerebellum may have played a key role in the emergence of human
81 cognition, including language(5).

82 A growing number of neuroimaging and clinical studies in humans also link cerebellar
83 structure and function to a wide range of cognitive and affective functions(6-8), as well as to a
84 number of heritable developmental(9) and psychiatric(10) disorders where these abilities either fail
85 to develop properly or are compromised later in life. However, compared to supra-tentorial brain
86 structures such as the cerebral cortex(11) and the hippocampus(12), few studies have mapped the
87 genetic architecture of the cerebellum.

88 Of note, the few existing cerebellar genome-wide association studies (GWAS) have mostly
89 been restricted to total cerebellar volume(13, 14), thus largely ignoring regional variation in cerebellar
90 morphology. Importantly, such variation in the relative volumes of cerebellar subregions (i.e.,
91 variation in cerebellar shape independent of total cerebellar volume) has been associated with
92 variation in behavioral repertoires in several species(15, 16), including domain-general cognition in
93 primates(16).

94 We here performed a GWAS of MRI-derived regional cerebellar morphological features in a
95 large population-based sample from the UK biobank (n discovery = 27,302; n replication:11,264),
96 functionally characterized the genetic signal, tested for enrichment of SNPs and genes linked to
97 human evolution, and assessed genetic overlap with major mental disorders.

98
99

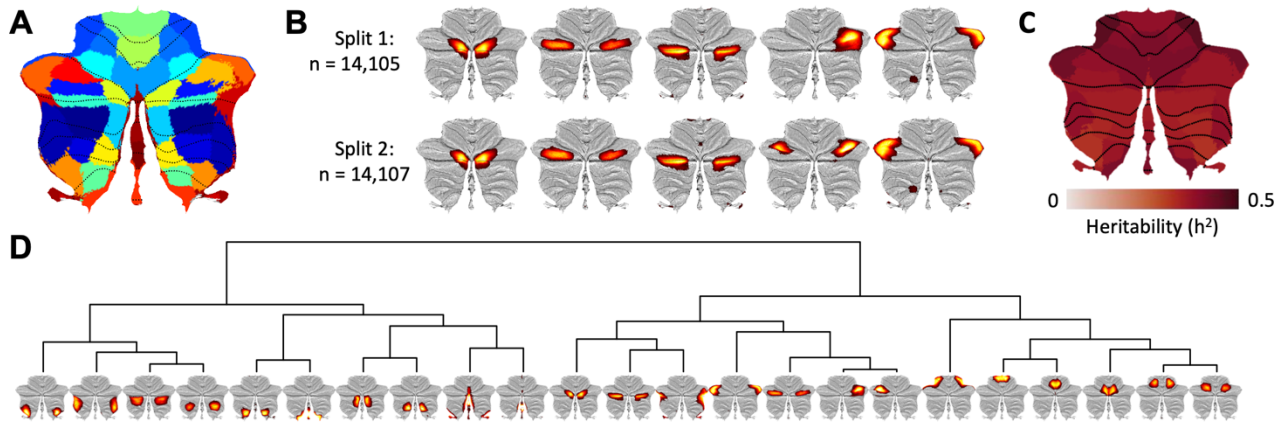
100 Results

101

102 **Data-driven decomposition of cerebellar grey matter maps reveals highly reproducible** 103 **morphological features.**

104 Since traditional atlases of the cerebellar cortex based on gross anatomical landmarks (i.e., lobules)
105 only partially overlap with more recent functional parcellations of the cerebellum(17-25), we first used
106 a data-driven approach (non-negative matrix factorization, NNMF(26-28)) to parcellate voxel-based
107 morphometry (VBM) based maps of cerebellar grey matter volume from 28,212 participants into
108 robustly reproducible sub-regions. NNMF yielded highly reproducible decompositions (across split-
109 half datasets) for model orders (i.e., number of components specified) ranging from 2 to 100 (see
110 Online Methods for details about the study sample, MRI processing and quality control procedures).
111 After observing that the improved fit to the original data seen with higher model orders tended to

112 level off between 15 and 30 components (indicating that the intrinsic dimensionality of the data might
113 have been reached), we decided on a model order of 23 based on its good split-half reproducibility
114 (see Fig. 1B, Online Methods for details regarding model order selection, as well as Supplementary
115 Figure 1 for summary maps of all tested model orders).
116



117
118 **Figure 1: Data driven decomposition of cerebellar grey matter maps yields highly**
119 **reproducible and moderately heritable morphological features.** **A:** Binarized winner-takes-all
120 map for the 23-component solution based on data-driven decomposition of cerebellar grey matter
121 maps from 28,212 participants. Note that empirically derived boundaries between cerebellar regions
122 only partially follow traditional lobular borders (marked with dotted black lines); **B:** Five distinct
123 components overlapping cerebellar Crus I derived from the split-half reliability analyses. While one
124 of these components emerged as bilateral in Split 2, the remaining four components were almost
125 identical, despite being derived from two independent samples; **C:** Narrow sense (SNP-based)
126 heritability of the 23 components (see Supplementary Data 5 for numerical values). **D:** Hierarchical
127 clustering of the 23 components (derived from the full sample decomposition) based on their pairwise
128 genetic correlations revealed a primary division between the anterior and posterior cerebellum, with
129 additional separations between medial and lateral regions. The full genetic correlation matrix can be
130 found in Supplementary Data 6.

131
132 Of note, our data-driven decomposition differed markedly from the standard cerebellar atlas based
133 on gross anatomical features, shown as dotted lines in Fig 1A (see Supplementary Figure 2 for all
134 23 components and Supplementary Data 1 for quantification of overlap between NNMF-derived
135 components and standard cerebellar anatomical regions, i.e. lobules). For instance, five distinct
136 components overlapped Crus I of cerebellar lobule VII (shown in Fig 1B), an anatomical region which
137 already started to split into separate components at a model order of three. We further observed
138 only partial overlap with task-based functional parcellations of the cerebellar cortex (Supplementary
139 Data 2). While some components clearly overlapped cerebellar regions previously associated with
140 hand movements, eye-movements/saccades or autobiographical recall, other data-driven
141 components overlapped multiple functionally defined cerebellar regions (Supplementary Data 2).

142 **Cerebellar morphological features are heritable and reveals a distinct anterior-posterior**
143 **pattern based on their bivariate genetic correlations.**

144 After removal of one of each genetically related pair of individuals ($n = 910$), 27,302 participants
145 remained for the genetic analyses. In addition to the 23 regional cerebellar morphometric features
146 of primary interest, we also included total cerebellar volume, estimated total intracranial volume and
147 9 cerebral brain phenotypes to serve as covariates and/or comparison phenotypes. Prior to the
148 genetic analyses, all morphological features were adjusted for effects of scanner site, sex, age,
149 estimated total intracranial volume, 40 genetic population components, genetic analysis batch and
150 a quantitative structural MRI quality index (the Euler number(29)) using general additive models,
151 before finally being rank-order normalized (see Online Methods for details).

152 To validate our analysis approach, we computed genetic correlations (using LD-score
153 regression, LDSC(30)) between univariate GWAS results on the comparison features and previously
154 neuroimaging GWAS studies. Results showed a mean r_g of .90 (range: .80-.99, see Supplementary
155 Data 3). For the 23 cerebellar morphological features, we computed genetic correlations between
156 discovery ($n = 27,302$) and replication ($n = 11,264$) samples using LDSC(30). These genetic
157 correlations were high (mean r_G : .92; range: .83-1), indicating reliable genetic signals (see
158 Supplementary Data 4).

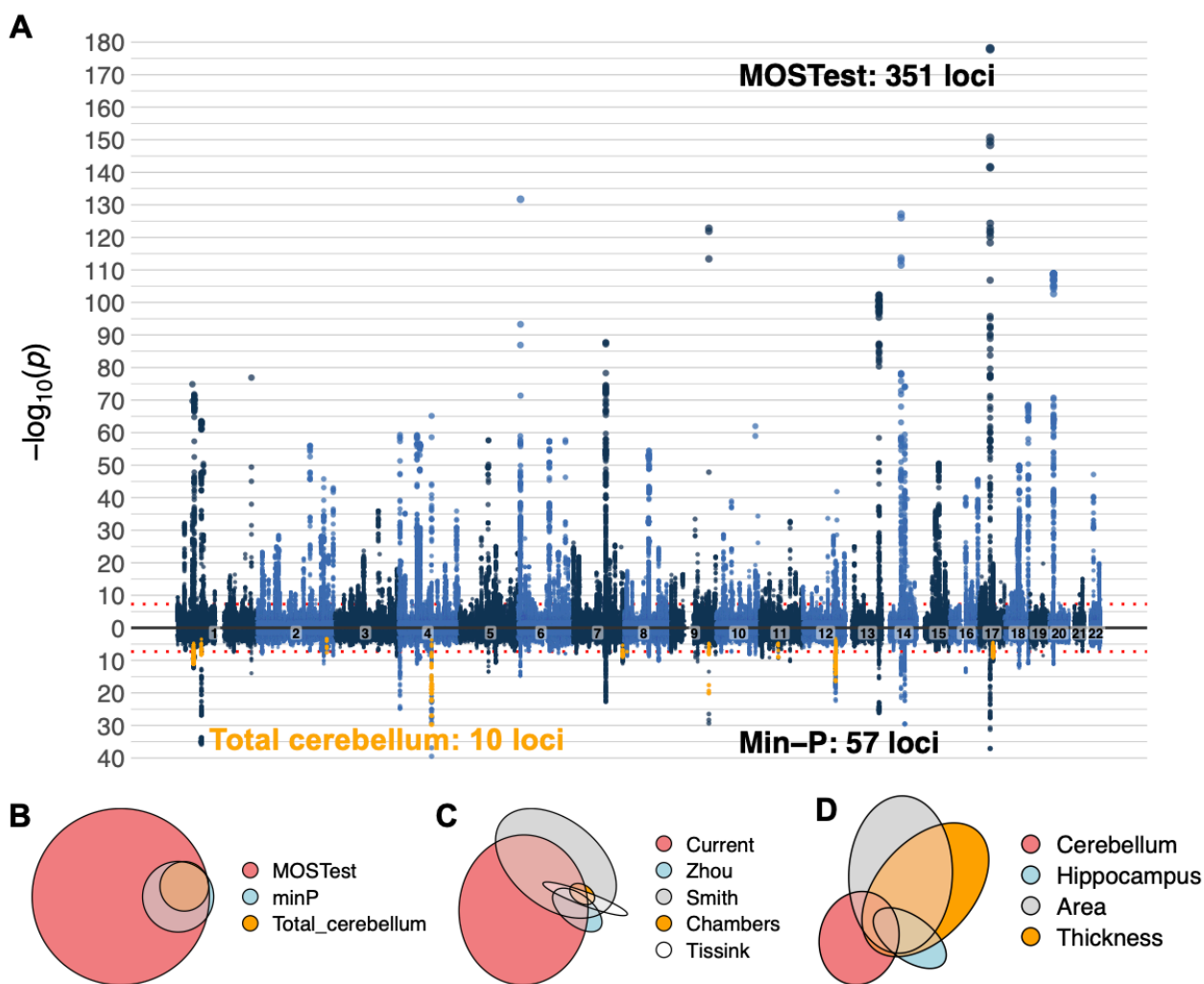
159 Genetic complex trait analysis (GCTA(31)) revealed SNP-based heritability estimates (h^2)
160 ranging from .33 to .44 (Figure 1C and Supplementary Data 5). Analyses of total cerebellar volume
161 ($h^2 = .35$), estimated total intracranial volume ($h^2 = .41$) and the 9 cerebral comparison phenotypes
162 (h^2 range: .26 to .45) gave a similar range of heritability estimates (Supplementary Data 5).

163 Hierarchical clustering of cerebellar features based on their bivariate genetic correlation
164 matrix (GCTA-based r_G ranging from 0.35 to 0.98, Supplementary Data 6) revealed a primary
165 anterior-posterior division running along the horizontal fissure separating Crus I and Crus II, with
166 secondary divisions grouping features into more lateral or medial, as well as more anterior and
167 posterior features within the major anterior and posterior regions (Fig 1D). Of note, the primary
168 division along the horizontal fissure was also evident from the (genetically naïve) two-component
169 NNMF decomposition, while medial-to-lateral divisions already began to emerge with a model order
170 of three (see Supplementary Figure 1).

171 In order to examine whether this phenotypic and genetic correlation structure was also
172 reflected in regional cerebellar gene expression patterns, we used the abagen toolbox(32) to extract
173 Allen Human Brain Atlas(33) gene expression profiles for 22 of the 23 morphological features and
174 computed their bivariate Pearson correlations (across 15,631 genes; Supplementary Data 7) and
175 hierarchical clustering solution (Supplementary Figure 4). The anterior-posterior boundary across
176 the horizontal fissure was also evident in the gene expression data, which in addition highlighted
177 distinct gene expression patterns for the posterior midline (grouped together with the horizontal
178 fissure), as well as for the most lateral regions of the cerebellar cortex.

179

180 **Multivariate GWAS reveals 351 genetic loci associated with cerebellar morphology.** Figure 2A
 181 shows the main results for the multivariate GWAS across the 23 cerebellar morphological features
 182 applying MOSTest(34). We observed 35,098 genome-wide significant (GWS) SNPs, which were
 183 mapped by FUMA(35) to a total of 51,803 candidate SNPs by adding reference panel SNPs in high
 184 LD ($r > .6$) with GWS SNPs. The 51,803 candidate SNPs (see Supplementary Data 8) were
 185 represented by 1,936 independent significant SNPs and 560 lead SNPs in 351 genomic loci (see
 186 Supplementary Data 10). The QQ-plot of the MOSTest results did not suggest inflation, while the
 187 QQ-plot of results based on permuted data (under the null hypothesis) confirmed the validity of the
 188 MOSTest analytical approach (Supplementary Figure 5).



189
 190 **Figure 2: Multivariate GWA analysis of the 23 cerebellar morphological features revealed 351**
 191 **independent genome-wide significant (GWS) loci.** **A:** The upper half of the Miami plot shows the
 192 main results from the multivariate analysis. The lower half displays results from a series of 23
 193 univariate analyses (corrected for multiple comparisons using the standard min-P approach), as well
 194 as results from a univariate analysis of total cerebellar grey matter (marked in orange). **B-D:** Euler
 195 diagrams showing the relative numbers of - and overlaps between - candidate SNPs mapped by the
 196 three analysis approaches employed in the current study (**B**), the current and four recent studies

197 *reporting genetic associations with cerebellar morphology (C), as well as results from multivariate*
198 *GWASs on hippocampal and cerebrocortical morphology (D).*

199

200 Annotation of all candidate SNPs using ANNOVAR(36) as implemented in FUMA³⁵ revealed that the
201 majority of candidate SNPs were intronic (57.8%) or intergenic (38.3%). While only 0.7% were
202 exonic, about 81% of the candidate SNPs were assigned minimal chromatin states between 1 and
203 7 (i.e., open chromatin states), implying effects on active transcription³⁷ (see Supplementary Data 8-
204 9).

205 We evaluated the robustness of these multivariate results using a multivariate replication
206 procedure established in Loughnan et al(37), which computes a composite score from the mass-
207 univariate z-statistics (i.e., applying multivariate weights from the discovery sample to the replication
208 sample input data) and then tests for associations between this composite score and genotypes in
209 the replication sample (for mathematical formulation see Loughnan et al(37)). Results showed that
210 97% of loci lead SNPs present in both samples replicated at a nominal significance threshold of $p <$
211 $.05$ (Supplementary Figure 6 and Supplementary Data 8), and that 74% remained significant after
212 Bonferroni correction for the 339 replication tests conducted (Supplementary Data 10). Moreover,
213 99% of loci lead SNPs showed the same effect direction across discovery and replication samples
214 (Supplementary Figure 6 and Supplementary Data 10). Thus, 329 (94%) of the 351 reported loci
215 were replicated.

216 In addition, we assessed the robustness of the multivariate patterns by computing bivariate
217 correlations between feature z-score vectors assigned to the discovery sample lead SNPs in an
218 independent multivariate GWAS (MOSTest) performed on the replication sample. These correlations
219 (restricted to the 339 loci lead SNPs present in both samples) were relatively high (mean $r: .70$, see
220 Supplementary Data 10 and Supplementary Figure 7). Figure 3 and Supplementary Figure 7 give
221 some examples of discovery and replication sample multivariate patterns projected back onto the
222 cerebellar cortex.

223 To compare our main multivariate MOSTest results to univariate approaches, the lower part
224 of the Miami plot in Figure 2A, and Figure 2B, displays results from a set of univariate GWASs on
225 the cerebellar morphological features (which yielded 8370 candidate SNPs and 57 genomic loci,
226 corrected for multiple comparisons using the min-P approach(38, 39)), as well as the 4044 candidate
227 SNPs and 10 significant loci resulting from the univariate GWAS on total cerebellar grey matter
228 volume (marked in orange). 52 of the 57 loci identified in the univariate analyses of regional
229 cerebellar features overlapped 55 of the 351 loci identified using the multivariate method, while 9 out
230 of 10 loci identified in the univariate analysis of total cerebellar volume were also identified in the
231 multivariate analysis. Thus, our multivariate analysis of regional cerebellar features increased the
232 locus yield ~35-fold relative to analyzing total cerebellar volume and ~6-fold relative to performing a
233 set of univariate analyses on the same regional features.

234 We next compared the current findings with previously reported genetic loci for cerebellar
235 morphology by extracting summary statistics from two recent GWAS studies using the UKBB sample
236 ($n = 19k(40)$ and $33k(41)$) that included regional cerebellar volumes among the full set of analyzed
237 brain imaging-derived phenotypes ($101(40)$ and $3,144(41)$, respectively), as well as two recent
238 GWASs on total cerebellar volume ($n = 33k(13)$ and $27k(14)$, respectively). Candidate SNPs and
239 independent GWS loci were identified in FUMA using the same settings as for our primary analyses
240 and employing a liberal p -value threshold of $5e-8$ (i.e., not correcting for the total number of brain
241 imaging features analyzed). Results are displayed in Figure 2c and Supplementary Data 8 and 10.
242 In brief, we found that 19,527 of the 51,803 candidate SNP (i.e., 36%) and 123 of the 351 identified
243 genomic loci (i.e., 35%) overlapped with candidate SNPs and loci extracted from these three
244 previous studies. Thus, 228 of the 351 (i.e., 65%) genetic loci reported here are novel to the literature
245 on of cerebellar morphology genetics (see Supplementary Data 10).

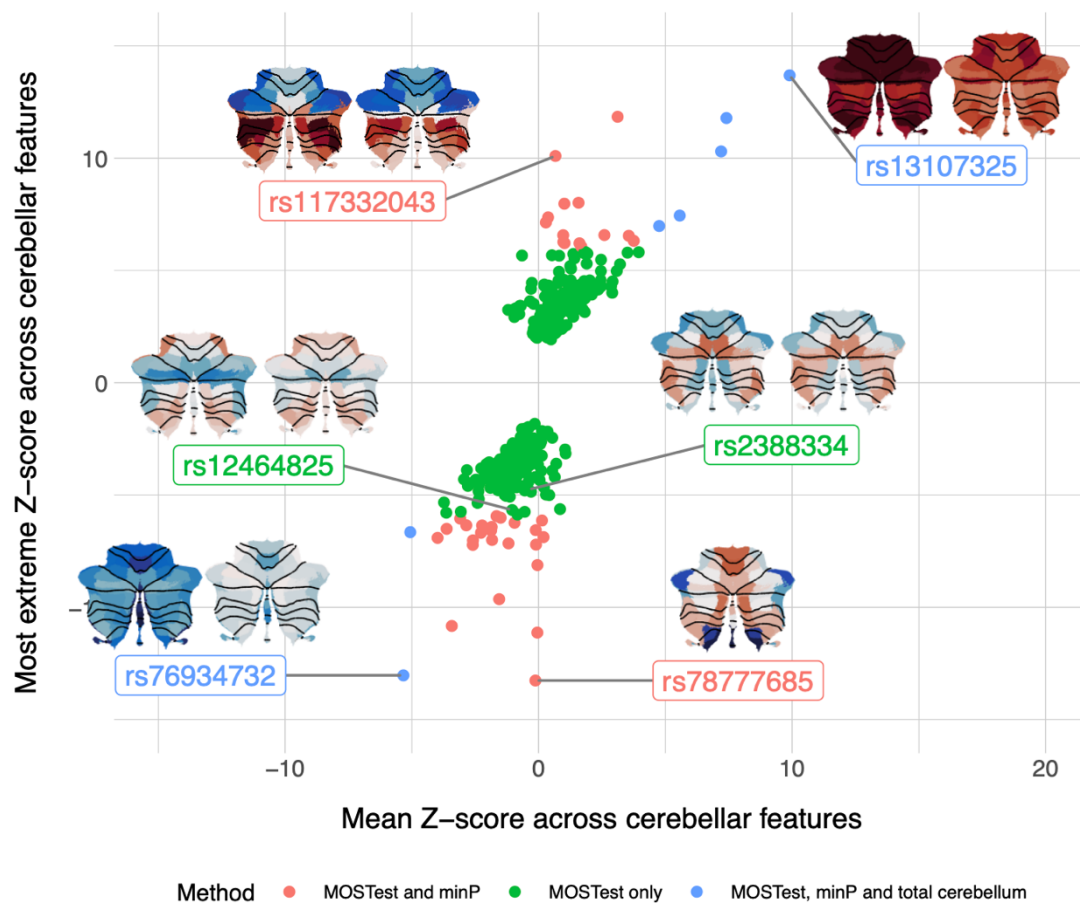
246 Overlap of cerebellar candidate SNPs and genetic loci with results from recent multivariate
247 analyses of hippocampal and cerebrocortical morphology are displayed in Figure 2D and
248 Supplementary Data 8 and 10 (final columns). Of note, we found that 32 and 29 percent of the
249 candidate SNPs discovered here for the cerebellum overlapped with candidate SNPs for vertex-wise
250 cerebrocortical surface area and thickness(42), respectively, while 11.4 percent overlapped with
251 candidate SNPs found for hippocampal subregions(43). 95 of the 351 genetic loci overlapped loci
252 linked to the other multivariate brain phenotypes (Supplementary Data 10). Thus, 64% of the
253 candidate SNPs and 73% of genetic loci appeared to be specifically associated with cerebellar
254 morphology.

255

256 **Significant genetic variants show heterogeneous effects across the cerebellar cortex,**
257 **influencing both regional and total volumes.**

258 A major advantage of our multivariate analysis approach is its sensitivity to both highly localized and
259 more generally distributed effects of SNPs on cerebellar morphology. This is illustrated in Figure 3,
260 which displays the 351 loci lead SNPs as a function of both the most extreme individual Z-score
261 across all cerebellar features (e.g, analogous to the strongest “local” effect) and of the mean Z-score
262 across these features (i.e. analogous to the main effect on overall cerebellar volume).

263



264

265

266

267

268

269

270

271

272

273

274

275

276

277

278

279

280

281

282

283

Figure 3: Lead SNPs show spatially heterogeneous – and replicable - effects across the cerebellar cortex. The 351 loci lead SNPs identified by MOSTest are plotted as a function of main overall effect across all cerebellar features (x-axis: mean Z-score) and most extreme effect for any single cerebellar feature (y-axis: most extreme Z-score across features), and colour coded by SNP discovery method. The cerebellar flat-maps show discovery (left) and replication (right) sample regional distributions of Z-scores (color-scale range from -10 to 10) for a few selected lead SNPs (see Supplementary Data 10 for individual feature Z-scores for all 351 discovery sample loci lead SNPs). SNP rs78777685 was only present in the discovery sample.

As can be seen, some lead SNPs (e.g. rs13107325; rs76934732) show pronounced positive or negative mean z-scores, indicating a relatively consistent direction of effect across cerebellar features. See also inset figures displaying feature Z-scores projected back onto the cerebellar cortex. Many of these SNPs also emerged in the univariate analysis of total cerebellar volume and were recently reported in GWASs on total cerebellar volume(13, 14).

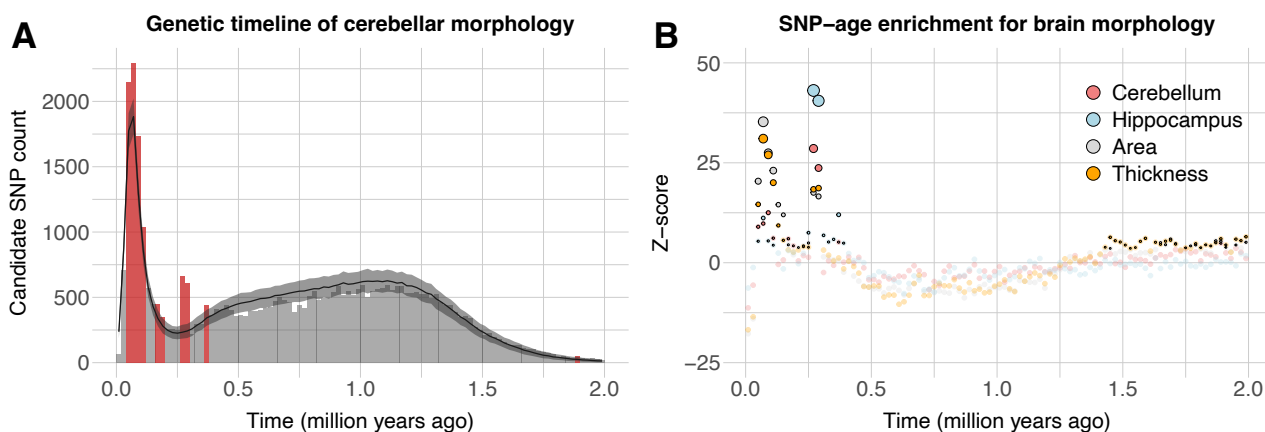
Many other lead SNPs, however, show strong “local” signals with opposite effect directions across features, yielding very weak global signals (e.g. rs117332043; rs78777685). Thus, while several of the most significant SNPs in this category have previously been reported in GWASs including local cerebellar morphological features(40, 41), they did not emerge from analyses of total cerebellar volume, neither in the current nor in previous studies.

284 Finally, our multivariate MOSTest approach is also sensitive to SNPs displaying weaker
285 effects distributed across several cerebellar features, often with opposite effect directions (e.g.
286 rs12464825; rs2388334). For this category of SNPs, neither of the univariate methods have sufficient
287 power at the current sample size. In contrast, these two example SNPs robustly emerged from the
288 multivariate analysis (discovery sample p-values < 1e-56; replication sample p-values < 1e-15).

289

290 **Genetic variants associated with cerebellar morphology are enriched for evolutionary recent** 291 **mutations in the human genome**

292 We next mapped the evolutionary age of cerebellar candidate SNPs by merging them with a recently
293 published dataset on dated mutations in the human genome(44). Following the analysis procedure
294 established by Libedinsky et al.(45), we plotted the histogram of dated candidate SNPs over the last
295 2 million years in bins of 20,000 years (Figure 4A and Supplementary Data 11), and tested for
296 positive or negative enrichment by comparing them to empirical null distributions derived from 10,000
297 randomly drawn and equally sized sets of all SNPs in the full human genome dating dataset (after
298 matching them to brain-related SNPs in terms of minor allele frequency; see Online Methods for
299 details).



300

301 **Figure 4: Genetic variants associated with cerebellar morphology are enriched for**
302 **evolutionary recent mutations in the human genome. A:** Histogram of estimated SNP age
303 (ranging from 0 to 2 million years, in bins on 20,000 years) for 41,549 candidate SNPs associated
304 with cerebellar morphology. The solid black line and grey ribbon denote the mean and Bonferroni-
305 corrected 95% confidence intervals derived from a null model constructed from 10,000 of equally
306 sized sets of SNPs randomly drawn from the Human Genome Dating Atlas of Variant Age (after
307 matching these to brain-related SNPs in terms of minor allele frequencies). Red bars denote time-
308 bins of significant positive enrichment. **B:** Enrichment Z-scores (calculated from means and standard
309 deviations of the corresponding null models) for candidate SNPs associated with cerebellar,
310 hippocampal and cerebrocortical surface area and cortical thickness morphology. Time bins with
311 significant positive enrichment are highlighted and marked with black borders, while circle size reflect
312 z-score (see Supplementary Data 11-12 for full numerical results).

313

314 Results revealed two main peaks of positive enrichment, the most prominent ranging from 260-300k
315 years ago (enrichment z-scores ranging from 23.7-28.6; see Figure 4B and Supplementary Data 11)
316 , i.e., coinciding with the emergence of anatomically modern humans (46, 47). The second strongest
317 enrichment peak (z-score range: 6.1-12.5) ranged from 40-120k years ago, i.e., overlapping the
318 human migration out of Africa, as well as the first evidence of several uniquely human behaviors
319 (often referred to as behavioral modernity), such as tool-making, recording of information onto
320 objects and purposeful burials(48).

321 For comparison, Figure 4B also shows results from analyses on candidate SNPs identified
322 in previous multivariate GWAS studies of hippocampal(43) and cerebrocortical(42) morphology.
323 These brain features also showed significant enrichment peaks, partially overlapping the cerebellar
324 results. Specifically, SNPs associated with hippocampal morphology also displayed the most
325 prominent enrichment peak between 260 and 300k years ago, while SNPs linked to cerebrocortical
326 morphology (surface area and thickness) tended to show the most significant enrichment for more
327 recent time bins (i.e., 40-120k years ago, see full results in Supplementary Data 12).

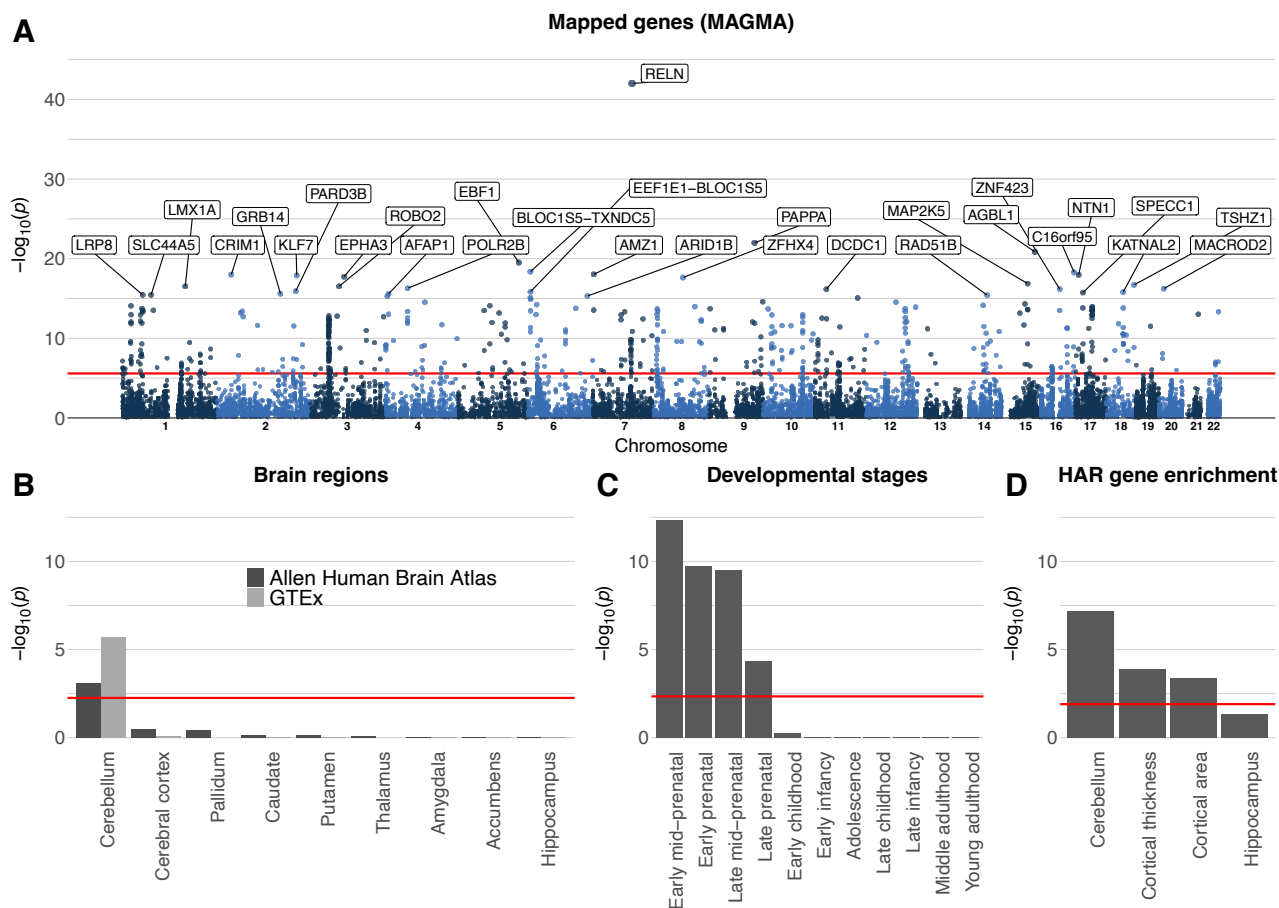
328

329 **Genes associated with cerebellar morphology show selective expression in cerebellar and**
330 **prenatal brain tissue, as well as enrichment for genes linked to human accelerated regions.**

331 To functionally characterize the multivariate GWAS signal, we mapped the full set of GWAS p-values
332 to 19,329 protein coding genes using MAGMA(49) and used the resulting gene-level p-values to test
333 for 1) GWS genes, 2) gene expression in brain tissue; and 3) enrichment for genes linked to human
334 accelerated regions (HARs), i.e. sections of DNA that have remained relatively conserved
335 throughout mammalian evolution, before being subject to a burst of changes in humans since
336 divergence of humans from chimpanzees(50, 51). These analyses yielded a total of 534 GWS genes
337 (i.e., 2.78% of all protein coding genes, see Figure 5A and Supplementary Data 13). Using the full
338 set of 19,329 gene-level p-values in MAGMA gene property analyses revealed significant and
339 specific gene expression in cerebellar and prenatal brain tissue (Figure 5B-C and Supplementary
340 Data 14-15), with the selective cerebellar expression seen in two independent datasets (Allen
341 Human Brain Atlas(33) and The Genotype-Tissue Expression (GTEx) Project).

342 The MAGMA gene set analysis of HAR-linked genes revealed significant enrichment ($p =$
343 $7.09e-08$) for genes associated with cerebellar morphology (Figure 5D, Supplementary Data 16). Of
344 note, running this same HAR gene set analysis on summary statistics from recent multivariate GWAS
345 studies on cerebrocortical(42) or hippocampal(43) morphological features yielded similar (for cortical
346 features) or significantly weaker (hippocampal features) enrichment effects (Figure 5d, see Online
347 Methods for processing pipeline).

348



349

350

351

352

353

354

355

356

357

358

359

360

361

362

363

364

365

366

367

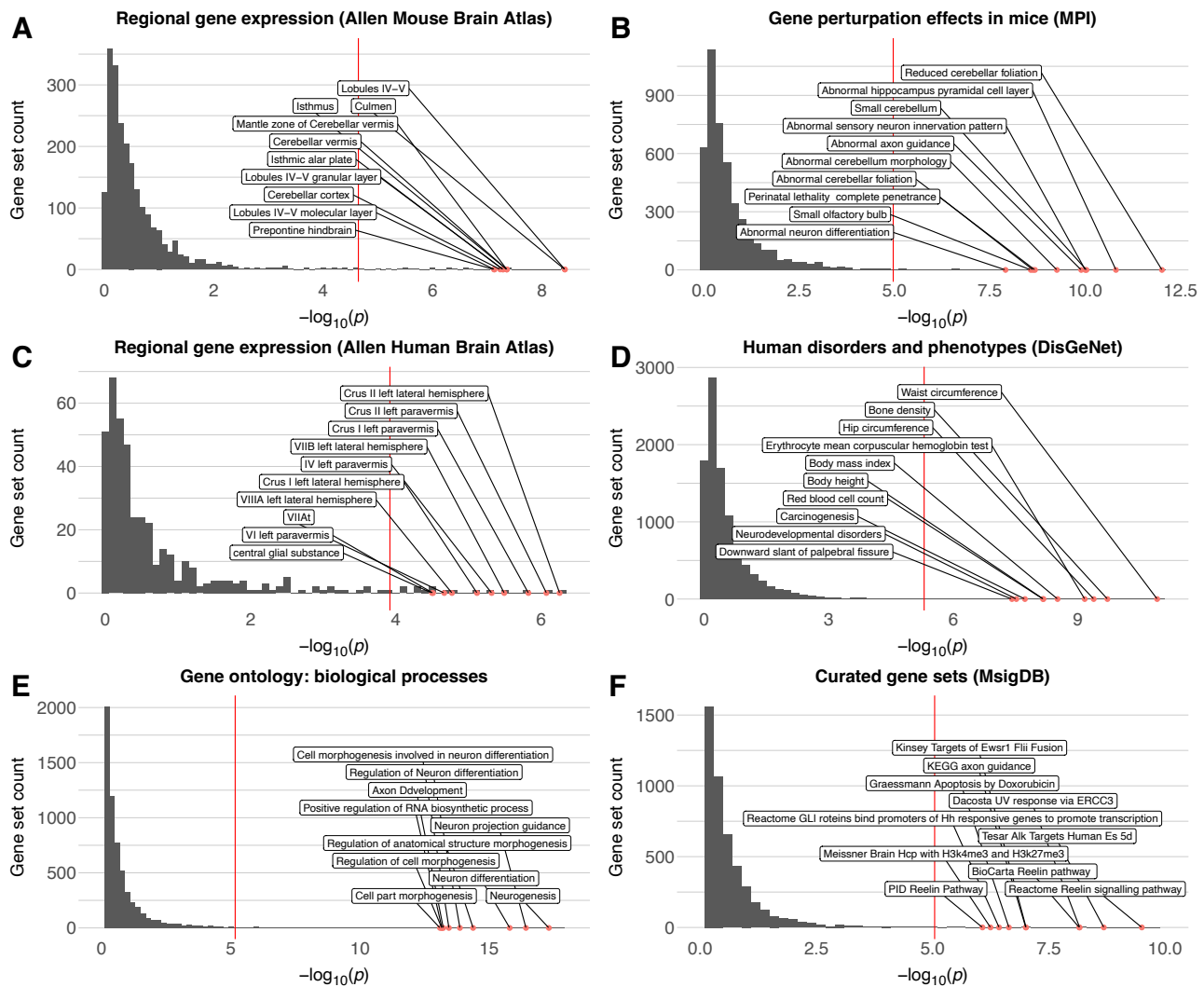
368

369

Figure 5: Gene mapping reveals selective enrichment for cerebellar and prenatal brain tissue, as well as for genes linked to human accelerated regions. **A:** MAGMA mapped the full range of SNPs from the multivariate GWAS to 19,329 protein-coding genes, 534 of which were genome-wide significant (Bonferroni corrected threshold marked with red line), with the 30 most significant genes labeled in the gene-based Manhattan plot. **B-C:** MAGMA gene-property analyses revealed selective brain expression in the cerebellum and during prenatal developmental stages. **D:** MAGMA gene-set analysis revealed significant enrichment for sets of genes previously linked to human accelerated regions (HARs). Figure 4d also shows results from comparative analyses using summary statistics from other multivariate GWASs of MRI-based brain, as well as significant results from statistical tests comparing beta-weights for HAR-linked genes across multivariate brain features. Horizontal red lines mark the Bonferroni-corrected significance threshold for each subplot. See Supplementary Data 13-16 for full results.

Genes linked to human cerebellar morphology show enrichment for gene sets linked to selective cerebellar gene expression, altered cerebellar morphology in mouse models, human clinical/anthropometric traits, as well as specific biological processes and pathways. In line with the continuous brain tissue gene expression results described above, we also observed significant and relatively selective enrichment for smaller curated sets of genes previously found to be highly and selectively expressed in mouse (Figure 6A, Supplementary Data 17) and human (Figure 6C, Supplementary Data 19) cerebellar brain tissue, as well as for sets of genes previously

370 shown to affect cerebellar morphology in mouse gene perturbation experiments (Figure 6B,
 371 Supplementary Data 18) and various clinical conditions and anthropometric traits in humans (Figure
 372 6D, Supplementary Data 20). The most significant gene ontology and curated gene sets from the
 373 MSigDB(52, 53) database were related to brain development (e.g., neurogenesis, axon guidance
 374 and neuron differentiation, Figure 6E, Supplementary Data 21), and highlighted the reelin signaling
 375 pathway (Figure 6F, Supplementary Data 22).
 376



377
 378 **Figure 6: Gene mapping reveals selective enrichment across brain tissues and curated gene**
 379 **sets.** MAGMA gene-set analyses revealed significant enrichment for sets of genes previously linked
 380 to preferential expression in human (A) and mouse (C) cerebellar tissue, as well as effects on
 381 cerebellar morphology (and other brain phenotypes) in mouse gene perturbation experiments (B)
 382 and human clinical disorders and phenotypes (D). Significant gene ontology terms were related to
 383 neural development (E), while curated gene sets highlighted the Reelin signaling pathway (F).
 384 Across all subplots the x-axis shows the $-\log_{10}(p)$ value, the y-axis marks the number of gene sets,
 385 and the top 10 most significant gene-sets are labelled. Red lines mark the Bonferroni-corrected
 386 significance threshold for each subplot. See Supplementary Data 17-22 for full results.
 387

388 As can be seen in Figure 5A (and Supplementary Data 13), *RELN* (encoding the protein Reelin) was
389 also the most significant gene mapped by MAGMA. See also Supplementary Figure 8 for a regional
390 locus plot showing the 12 lead SNPs mapped to *RELN* and their associated z-score maps.

391

392 **Gene mapping reveals sets of plausible causal genes**

393 In addition to the gene-based mapping strategy using all SNPs described above (MAGMA), we also
394 mapped candidate SNPs to genes using two complementary gene mapping strategies: 1) positional
395 mapping of deleterious SNPs (defined as having a CADD-score⁽⁵⁴⁾ > 12.37); and 2) mapping of
396 SNPs previously shown to affect gene expression in cerebellar tissues (i.e., eQTL mapping). Across
397 all three strategies, we mapped a total of 674 unique genes; 531 using MAGMA, 310 using positional
398 and 197 using eQTL mapping (see Figure 7A and Supplementary Data 23). 298 genes were
399 identified by at least two strategies, while 65 genes were mapped by all three strategies. Out of these
400 674 genes, 61 have previously been associated with cerebellar pathology in humans and/or altered
401 cerebellar morphology in mouse gene perturbation experiments, while 121 have been linked to
402 human accelerated regions (Supplementary Data 23). As can be seen in Figure 7B and
403 Supplementary Data 23, the 674 genes mapped to cerebellar morphology showed some overlap
404 with genes mapped to hippocampal⁽⁴³⁾ and cerebrocortical⁽⁴²⁾ morphology using the same
405 mapping strategies, but 264 genes (39%) appeared relatively specific to the cerebellum.

406 Results from gene set analyses on the 674 mapped genes (Figure 7, Supplementary Data
407 24-28) largely mirrored results from the MAGMA analyses described above, but in addition revealed
408 that this set of 674 mapped genes was also enriched for gene sets associated with several complex
409 clinical phenotypes and anthropometric traits in humans, including cognitive ability, neuroticism and
410 schizophrenia (Figure 7F, Supplementary Data 28).

411 Of note, while the full set of mapped genes showed significant enrichment for sets of genes
412 known to alter cerebellar morphology in mouse mutation or knock-down experiments
413 (Supplementary Data 26), we also note that 613 of the 674 mapped genes have not to our knowledge
414 previously been linked to cerebellar development, anatomy or pathology in mice or humans
415 (Supplementary Data 23), and thus constitute potential targets for future gene perturbation
416 experiments in animal models.

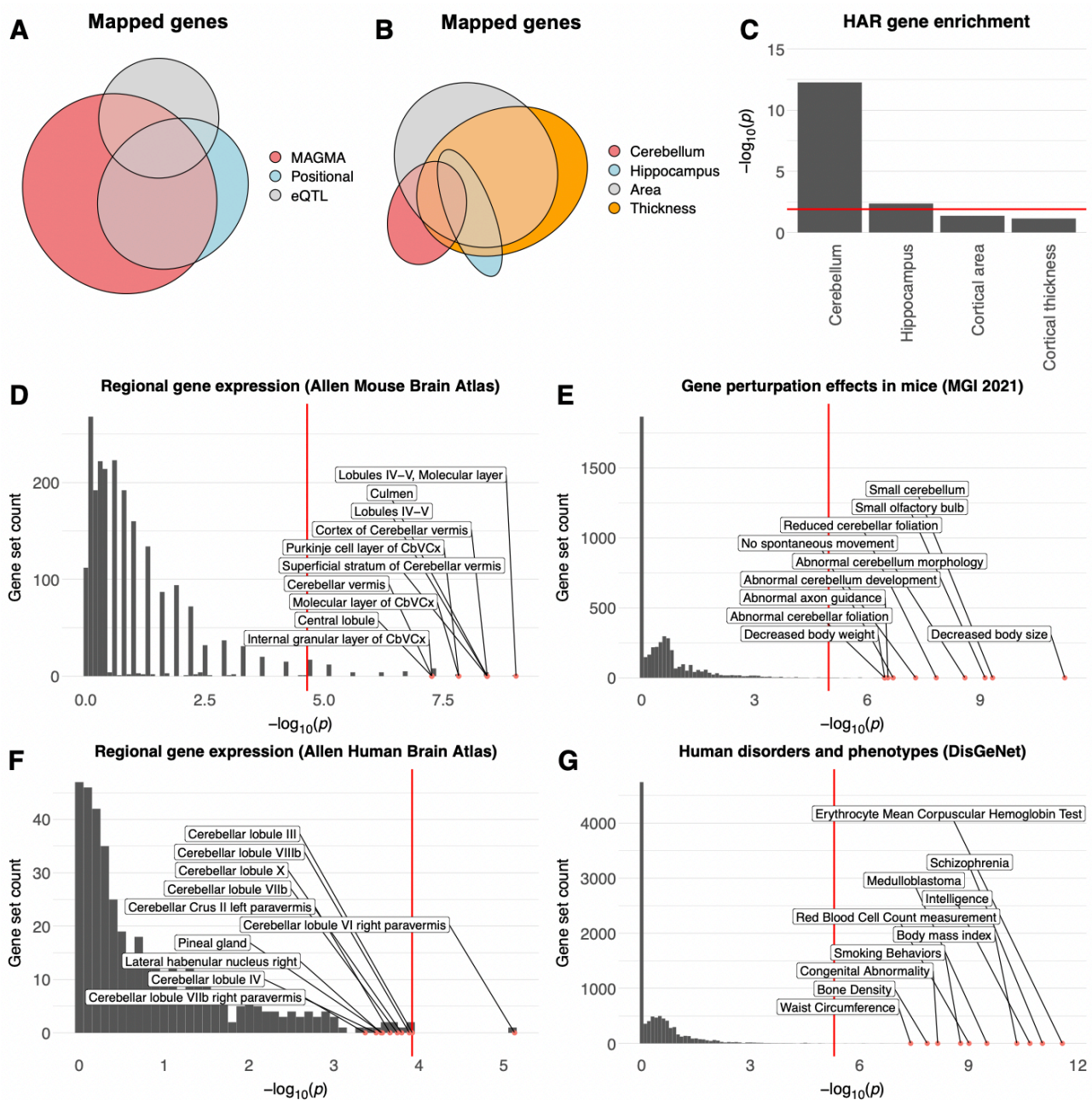
417 Restricting the above analyses to the 298 genes mapped across at least two strategies did
418 not markedly affect the results (Supplementary Data 24-28, final columns).

419

420

421

422



423

424

425

426

427

428

429

430

431

432

433

434

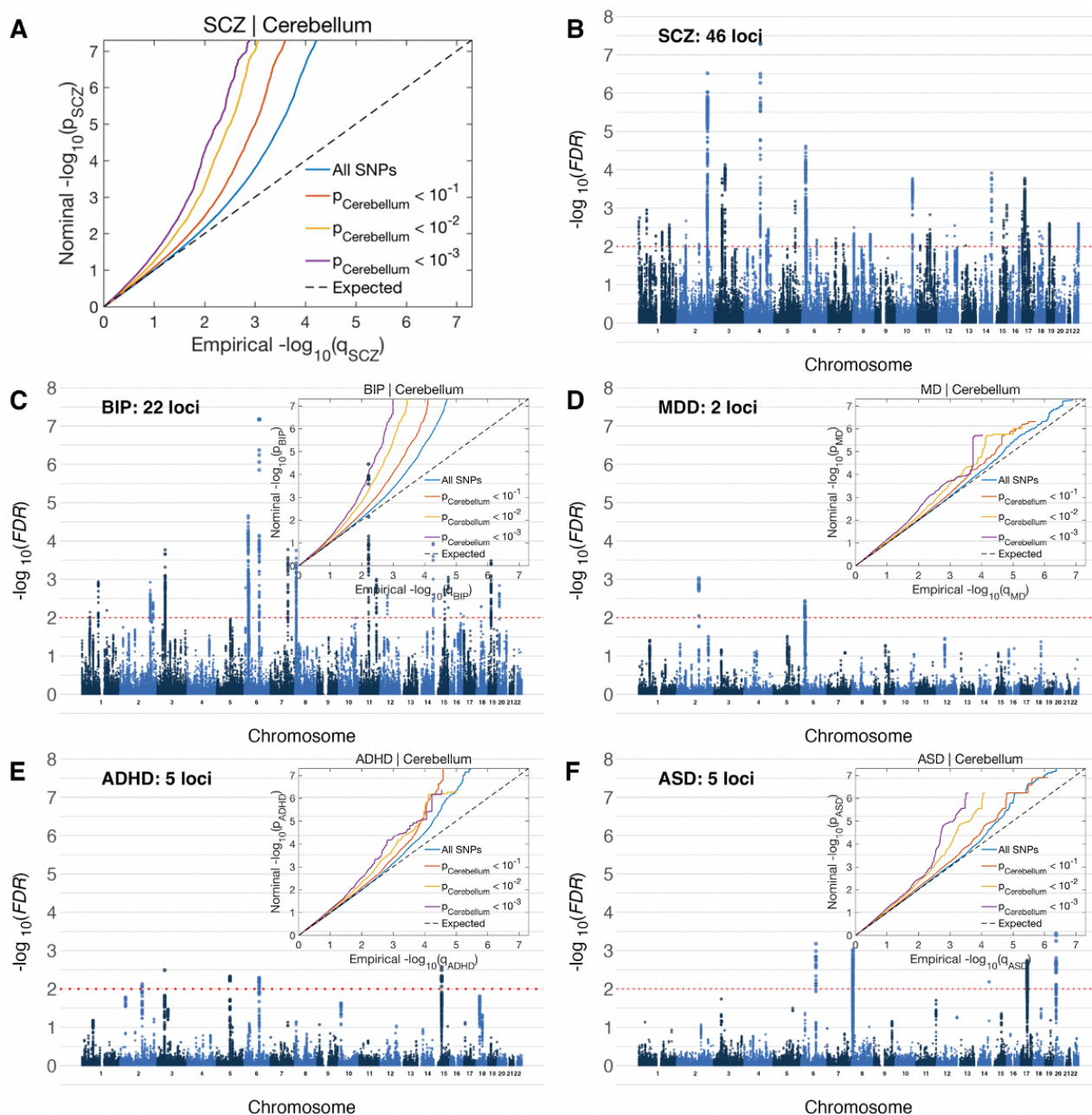
435

Figure 7: Mapping and functional characterization of plausible causal genes. The 674 plausible causal genes mapped using three complementary strategies (A) show partial overlap with genes mapped to hippocampal(43) and cerebrocortical(42) morphology (B); significant enrichment for sets of genes linked to human accelerated regions (HAR) (C); selective expression in the cerebellum in mice (D) and humans (E), as well as effects on cerebellar morphology in mouse gene perturbation studies (F) and human disorders and anthropometric phenotypes (G). See Supplementary Data 23-28 for full results.

Cerebellar morphology shows significant genetic overlap with psychiatric disorders

We finally tested for overlap between the multivariate genetic profile for cerebellar morphology and genetic profiles for five major developmental/psychiatric disorders (attention deficit hyperactivity disorder: ADHD; autism spectrum disorder: ASD; bipolar disorder: BIP; major depressive disorder:

436 MDD; and schizophrenia: SCZ) using conditional/conjunctive FDR analysis(55). As can be seen
 437 in the conditional QQ-plots in Figure 8, these analyses revealed clear patterns of enriched
 438 association with the clinical phenotypes when selecting subsets of SNPs with increasingly stronger
 439 association with cerebellar morphology (Fig. 8A and figure insets in (C-F).



440

441 **Figure 8: Genetic variants influencing cerebellar morphology overlap with variants**

442 **associated with five major mental disorders.** Conditional QQ plots (A and figure insets in C-F)

443 show an incremental incidence of association with five mental disorders (leftward deflection) as a

444 function of the significance of association with cerebellar morphology. Manhattan plots show SNPs

445 with significant association with both traits, thresholded at a conjunctive FDR threshold of $p > .01$

446 (red dotted line). SCZ: Schizophrenia; BIP: Bipolar Disorder; MDD: Major Depressive Disorder;

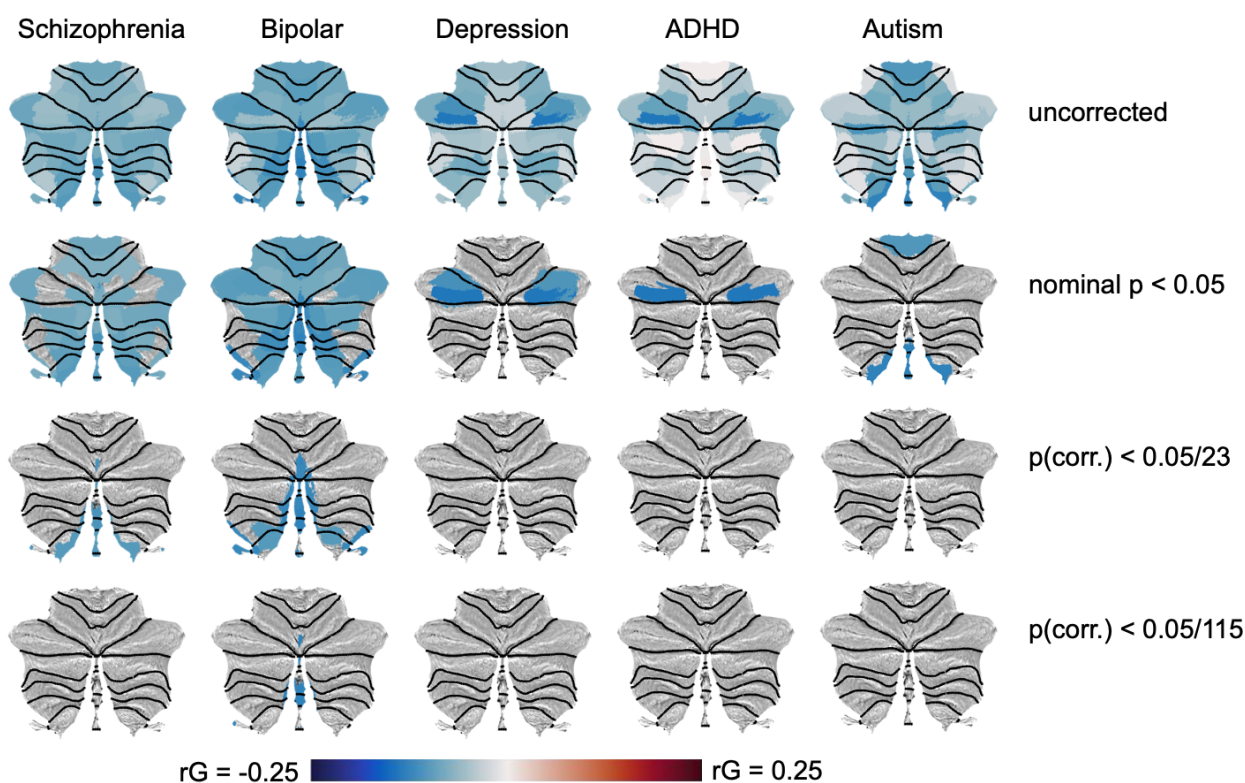
447 ADHD: Attention Deficit Hyperactivity Disorder; ASD: Autism Spectrum Disorders.

448

449 See also Supplementary Figure 9 for QQ-plots depicting the reverse association, i.e., enriched
450 association with cerebellar morphology when conditioning on the association with
451 developmental/psychiatric disorders. Specific genetic variants jointly influencing the two phenotypes
452 were identified using conjunctive FDR analyses at a conservative statistical threshold of $p < .01$.
453 Results revealed shared genetic loci with all disorders; namely 48 with SCZ, 22 with BIP, 2 with
454 MDD, 5 with ADHD and 5 with ASD (Figure 6; Supplementary Data 29-33). We mapped lead and
455 candidate SNPs for each of these loci to genes using positional and eQTL mapping and checked for
456 gene overlap across disorders (Supplementary Data 34). Of note, the *LRP8* gene (a HAR-linked
457 gene(50, 51) encoding a Reelin receptor) emerged from the conjunctive FDR analyses of both BIP
458 and SCZ, thus again highlighting the Reelin signaling pathway.

459 To complement these multivariate analyses, we also conducted a set of univariate analyses,
460 using LD-score regression(30) to calculate the genetic correlations between each individual
461 cerebellar feature and the five developmental/psychiatric disorders.

462



463

464 **Figure 9: Univariate genetic correlations between cerebellar morphological features and five**
465 **major mental disorders are negative.** The top row display unthresholded genetic correlations,
466 while these are filtered at increasingly strict statistical thresholds in the following rows, i.e. nominal
467 p -value $< .05$ (second row); Bonferroni correction for the 23 cerebellar features tested (third row);
468 and Bonferroni correction for both 23 features and 5 clinical conditions (bottom row). Black dotted
469 lines denote lobular boundaries.

470

471 As can be seen in the first row of Figure 9 (and Supplementary Data 35), genetic correlations with
472 cerebellar morphological features were predominantly negative across diagnoses, indicating that
473 genetic variants associated with a clinical diagnosis tended to also be associated with reduced
474 cerebellar volumes (with 42 out of 115 tested associations showing nominally significant negative
475 correlations; Fig 9, second row). However, all univariate genetic correlations were relatively weak,
476 and only a few negative genetic correlations with BIP and SCZ survived Bonferroni correction for the
477 23 features tested. When also correcting for the five clinical conditions, only the negative correlation
478 between BIP and cerebellar feature 23 (primarily overlapping vermal lobules VIIIa and VIIIb)
479 remained significant.

480 Supplementary Data 36 show genetic correlations between the five disorders and the ten
481 comparison brain phenotypes, as well as total cerebellar volume. In general agreement with the
482 observed pattern for regional cerebellar features, total cerebellar grey matter volume showed
483 nominally significant negative genetic correlations with BIP (rg: -.10; p = 0.0052) and SCZ (rg: -.09;
484 p = 0.0133). Pallidal volume also showed nominally significant negative genetic correlations with
485 these two disorders (BIP: rg: -.10; p = 0.0087; SCZ: rg: -.08; p = 0.0172, while ADHD displayed
486 negative genetic correlations with estimated total intracranial volume (rg: -.15; p = 0.0003) and total
487 cortical surface area (rg: -.14 ; p = 0.0065), as well as a positive genetic correlation with hippocampal
488 volume (rg: .13; p = 0.0164). Finally, MDD showed nominally significant negative genetic correlations
489 with volumes of the hippocampus (rg -.08; p = 0.025) and thalamus (rg: -.09; p = 0.0258). Only the
490 negative genetic correlation between ADHD and estimated total intracranial volume survived
491 Bonferroni correction across the 55 tests performed.

492

493

494 **Discussion**

495

496 The current study identified novel features of the genetic architecture of cerebellar morphology,
497 supported the notion of recent changes over human evolution, implicated specific neurobiological
498 pathways, and demonstrated genetic overlap with major mental disorders.

499 With respect to the main features of cerebellar morphology, it is worth noting that results from
500 our data-driven decomposition of cerebellar grey matter maps (which was not informed by genetic
501 data), the genetic correlation analyses of the chosen 23-feature solution and gene expression data
502 from the Allen Human Brain Atlas all converge on a similar general pattern. The first boundary to
503 emerge in the data-driven decompositions ran along the horizontal fissure separating Crus I and II
504 of lobule VII, reflecting its centrality in characterizing phenotypic variability in cerebellar morphology
505 at the population level. Of note, this boundary also emerged from clustering of the 23 cerebellar
506 morphological features based on their bivariate genetic correlations or gene expression profiles
507 (based on the Allen Human Brain Atlas). This latter finding essentially mirrors results from a recent
508 report using a different analysis strategy on the same gene expression data(56). Interestingly, the
509 horizontal fissure has been suggested to mark the border between two separate cerebellar

510 representations of the cerebral cortex, with a possible third representation in lobules IX-X(57). The
511 current cerebellar results thus complement previous work on the hierarchical genetic organization of
512 the cerebral cortex, which has identified the Rolandic fissure (separating the frontal and parietal
513 lobes) as a main boundary with respect to genetic effects of effects of surface area(58), as well as
514 a superior-inferior gradient for genetic influences on cortical thickness(59)

515 Our multivariate GWAS using MOSTest identified 351 independent GWS loci associated with
516 cerebellar morphology, increasing the yield ~35-fold relative to analyzing total cerebellar volume and
517 ~6-fold relative to performing a set of univariate analyses on the same regional features in our current
518 sample. 329 (94%) loci from the multivariate analyses were replicated in an independent sample,
519 indicating robust results. After applying a liberal threshold to summary statistics from previous well-
520 powered studies, we find that 228 (65%) of our reported loci are novel. Importantly, among the genes
521 mapped to these novel loci we find several that are known to play important roles in cerebellar
522 development in mice (e.g., *RORA*(60), *FGF8*(61) and *BAHRL1*(62), see Supplementary Data 22).
523 While candidate SNPs associated with cerebellar morphology partially overlap with SNPs previously
524 mapped to other multivariate brain phenotypes, we note that a substantial number of SNPs appear
525 to be relatively selectively linked to cerebellar morphology, a finding that is in line with the distinct
526 gene expression profile found for the cerebellum(33).

527 SNP- and gene-level results from the current study also bolster – and refine – the notion of
528 relatively recent changes in cerebellar morphology over human evolution(2, 4, 15, 16). Specifically,
529 we found that candidate SNPs associated with cerebellar morphology were particularly enriched for
530 SNPs with an estimated age of 260-300 thousand years, i.e., coinciding with the emergence of Homo
531 Sapiens(46, 47). Significant, but weaker, enrichment was also seen for time bins stretching from 40-
532 120 thousand years ago, i.e., overlapping the human migration out of Africa, as well as the first
533 evidence of several uniquely human behaviors (often referred to as behavioral modernity), such as
534 tool-making, recording of information onto objects and purposeful burials(48). Similar patterns of
535 enrichment was also found when analyzing candidate SNPs derived from previous studies on
536 multivariate hippocampal(43) and cerebro-cortical(42) morphology Gene level analyses further
537 showed that genes associated with inter-individual variation in cerebellar morphology are enriched
538 for genes linked to human accelerated regions (HARs)(50) of the genome. HARs denote previously
539 conserved regions of the genome that were subject to a burst of changes in humans after the
540 divergence of humans from chimpanzees about 6-8 million years ago(50). Of note, a recent GWAS
541 on total cerebellar volume found no enrichment for HAR-linked genes(14), suggesting that SNPs
542 associated with regional cerebellar variation may be driving this effect. While the comparisons with
543 cerebral features should be interpreted with care since different image preprocessing pipelines were
544 employed, it is nonetheless striking that HAR gene enrichment was nominally stronger for cerebellar
545 morphology than for vertex-wise cerebrocortical thickness and area, and significantly stronger than
546 for hippocampal regional volumes (Figure 5D).

547 Together, these SNP- and gene-level results suggest that genetic variants influencing
548 cerebellar morphology in modern humans have been subject to selection over relatively recent
549 human evolution, and that cerebellar changes – in concert with other brain regions - may thus have
550 played a central part in the emergence of uniquely human cognitive abilities.

551 Results from the MAGMA gene property and gene set analyses bolster our
552 confidence in the genetic signal by showing selective gene expression in human cerebellar brain
553 tissue across two independent datasets (Allen Human Brain Atlas and GTEx.8) and significant
554 enrichment for sets of genes which have previously been shown to affect cerebellar morphology in
555 mouse gene perturbation experiments. The MAGMA results further show significant enrichment for
556 sets of genes known to play key roles in neurodevelopment (e.g., neurogenesis & axon guidance)
557 and preferential expression in prenatal brain tissue, thus supporting a primarily developmental origin
558 of genetically determined effects on adult cerebellar morphology. Of note, our MAGMA enrichment
559 analysis of curated gene sets strongly implicated the Reelin signaling pathway. Indeed, both the
560 gene coding for the Reelin protein (*RELN*) and genes coding for its two receptors (*LRP8* & *VLDLR*)
561 were identified across at least two gene mapping strategies, with *RELN* emerging as the single most
562 significant gene by MAGMA. The Reelin pathway is known to play important roles in
563 neurodevelopment (e.g. neuronal migration), and mutations in the *RELN* and *VLDLR*(63) (and to a
564 lesser extent *LRP8*; also known as *ApoER2*(64)) have been associated with cerebellar
565 malformations and/or dysfunction. *LRP8* is also among the genes linked to human accelerated
566 regions (HARs) of the genome.

567 The sets of genes mapped by the three complementary mapping strategies provide a
568 database for future studies investigating the genetic architecture of cerebellar morphology. For
569 instance, we mapped 616 genes associated with inter-individual variability in human cerebellar
570 morphology that have not yet to our knowledge been examined in mouse gene perturbation
571 experiments and/or associated with cerebellar pathology in humans. Among these, we highlight
572 *MAP2K5* and *GRB14*, two HAR-linked genes mapped across all strategies and associated with lead
573 SNP p-values <1e-50, but whose functions in the brain are largely unknown.

574 The reported results for previously discovered variants, loci and genes add important
575 information regarding regional effects on cerebellar morphology. For instance, while genetic variants
576 linked to the *RELN* gene have previously been associated with volumes of cerebellar vermal lobules
577 VI-X and hemispheric lobule IX(40, 41), we here mapped 12 lead SNPs to *RELN* showing
578 heterogeneous effects across the entire cerebellar cortex (but with peak effects overlapping
579 previously described midline and posterior cerebellar regions, see Supplementary Figure 8).

580 The observed genetic overlap between cerebellar morphology and the five mental disorders
581 reinforces the recent notion of the cerebellum as a key brain structure in complex clinical traits and
582 disorders(6-10). Across the five diagnoses, the strongest evidence for genetic overlap with cerebellar
583 morphology was found for SCZ and BIP, likely at least in part because these disorder GWASs were
584 relatively well-powered. While an in-depth discussion of genetic loci jointly influencing psychiatric

585 disorders and cerebellar morphology is beyond the scope of this report, we note that the Reelin
586 pathway again emerges in the genetic overlap analyses for SCZ and BIP. Specifically, the current
587 finding of *LRP8* (a reelin receptor, and HAR-linked gene) as one of the genes jointly associated with
588 cerebellar morphology and the aforementioned severe mental disorders points towards a potential
589 molecular pathway involved in the cerebellar abnormalities previously reported in SCZ(10, 65, 66)
590 and BIP(65, 66). Indeed, in line with its key importance for brain development and function, the
591 Reelin pathway is also increasingly seen as relevant for a wide range of neurodevelopmental,
592 psychiatric and neurodegenerative disorders(67). Of particular relevance to the current findings,
593 converging evidence supports *LRP8* as a key susceptibility gene for psychosis(68).

594 The main limitations of the current study concern the ancestral homogeneity of the sample,
595 the sample size and the exclusion of very rare genetic variants. Limiting the sample to participants
596 of European ancestry was deemed necessary considering the current state of the multivariate
597 GWAS methods used but may limit the generalizability of our findings. Second, while the current
598 sample size is large in comparison with previous imaging genetics studies, it is still relatively small
599 in comparison to GWASs of other complex human phenotypes (e.g., intelligence, with a current n of
600 > 3 million(69)). Finally, very rare genetic variants (MAF < 0.005) were excluded from the current
601 multivariate GWAS, but are likely to include a number of variants with relatively large effect sizes on
602 complex human traits (70). Thus, future studies using larger and more diverse samples – as well as
603 whole exome and/or genome sequencing - are likely to discover more of the genetic variants
604 associated with cerebellar structure.

605 In conclusion, the current results enhance our understanding of the genetic architecture of
606 human cerebellar morphology, provide supporting evidence for cerebellar morphological changes
607 during the last ~6-8 million years of human evolution, and reinforce the notion of cerebellar
608 involvement in several mental disorders by demonstrating significant genetic overlap.

609
610
611
612
613
614
615
616
617
618
619
620
621
622

623

624

625 **Materials and Methods:**

626

627 **Participants**

628 For our main analyses, T1-weighted MR images, demographic and genetic data from 39,178 UK
629 Biobank participants were accessed using access number 27412. After removing 1043 participants
630 who either had missing genetic data or had withdrawn consent (as of 19.11.2019), data from 38,135
631 participants remained for the main analysis (age range: 44.6-82.1; mean age: 64.1, 51.9% female).
632 Following quality control procedures (QC, see below), 28,212 UK Biobank participants of European
633 descent remained for the main analyses (age range: 45.1-82.1; mean age: 64.1, 55.1% female), 910
634 of which were identified as close relatives and removed prior to genetic analyses (see below), leaving
635 a final sample for the primary analyses of 27,302 (age range: 45.1-82.1; mean age: 64.1, 54.9%
636 female). For the replication sample, we accessed a newer release of UK Biobank participants (n =
637 48,045) and removed the 27,302 participants included in the primary analyses. After running through
638 identical QC procedures as for the main sample (although applied only to the cerebellar features of
639 primary interest and covariates included when analyzing these), the replication sample consisted of
640 11,264 unrelated UK Biobank participants of European descent (age range: 46.1-83.7; mean age:
641 66.8, 46.9% female). The UK Biobank was approved by the National Health Service National
642 Research Ethics Service (ref. 11/NW/0382),

643

644 **Initial MR image processing**

645 MRI data was first processed using the recon-all pipeline in Freesurfer 5.3(71), yielding a large
646 number of brain features. Of these, we retained measures of estimated total intracranial volume
647 (eTIV), total cerebro-cortical surface area, average cerebro-cortical thickness as well as the volumes
648 of seven subcortical structures (hippocampus, amygdala, thalamus, pallidum, putamen, caudate
649 nucleus and nucleus accumbens) as cerebral (or global, in the case of eTICV) comparison regions
650 for our main cerebellar analyses. These anatomical features were averaged across hemispheres,
651 yielding a total of ten comparison phenotypes.

652 Next, the bias-field corrected T1-images from the FreeSurfer analyses were analyzed using
653 the cerebellum-optimized SUIT-toolbox(72). In brief, SUIT isolates the cerebellum and brain stem
654 from T1-images, segments cropped images into grey and white matter, and normalizes these tissue
655 probability maps to a cerebellum-specific anatomical template. After multiplying the grey matter
656 maps with the Jacobian of the transformation matrix (i.e. preserving information about absolute
657 volumes), we extracted grey matter intensity values overlapping the 28 cerebellar lobular labels in
658 the probabilistic SUIT-atlas. Since cerebellar volumetric indices showed high correlations across the
659 two hemispheres (range: .87-.96; mean: .94), we created mean volumetric measures by averaging
660 across hemispheres. Finally, we also combined the two smallest regions in the SUIT-atlas (Vermis

661 Crus I and II located in the midline, average volumes: 2.9 and 293.4 mm², respectively) to create a
662 new Vermis Crus region (average volume: 296.2 mm²). This procedure reduced the 28 cerebellar
663 lobular volumes to 16 morphological indices. Total cerebellar grey matter volume was defined as the
664 sum of all 28 lobular labels in the SUIT-atlas.

665

666 **Quality control procedures**

667 After excluding 4,818 UKBB participants of non-European origin, anatomical indices from the
668 remaining 33,317 participants went through an iterative quality control (QC) procedure. First, we
669 excluded 639 subjects with a mean Euler number below -217, indicating poor MRI quality(29), as
670 well as 12 subjects with missing and 90 subjects with zero values for any of the key cerebellar or
671 cerebral brain measures of interest. Next, we used general additive models (GAM, implemented in
672 the R-package “mgcv”) in order to model the effects of age (estimated as smooth functions for males
673 and females separately, using cubic splines with 10 knots), sex, and scanner site on estimated total
674 intracranial volume (eTIV) and mean thickness of the cerebral cortex. Specifically, we used the
675 following formula:

676

```
677     GAM_model<-gam(Anatomical feature ~ s(Age, bs = “cs”, by = Sex, k = 10) + as.factor(Sex)  
678     + as.factor(Scanner), data = UKBB_cerebellum_GWAS, select = TRUE, method = “REML”)
```

679

680 Adjusted eTIV and mean cortical thickness indices were then created by reconstructing the data
681 using the intercept and residuals from this model (i.e., removing effects of age, sex and scanner),
682 before identifying and rejecting potential outliers, defined as +/- 3 median absolute deviations
683 (MAD)(73) from the median of these adjusted values. Data from 350 subjects were rejected based
684 on these criteria.

685 For the remaining cerebral anatomical measures, as well as total cerebellar volume, this
686 procedure was then repeated, with scaled eTIV as an additional predictor. Since previous studies
687 have demonstrated that the relationship between regional brain volumes and intracranial volume is
688 not strictly allometric(74, 75), we estimated the effect of eTIV using cubic splines with 10 knots.
689 Specifically, we used the following formula:

690

```
691     GAM_model<-gam(Anatomical feature ~ s(Age, bs = “cs”, by = Sex, k = 10) + as.factor(Sex)  
692     + as.factor(Scanner) + s(eTIV_scaled, bs = “cs”, k = 10), data = UKBB_cerebellum_GWAS,  
693     select = TRUE, method = “REML”)
```

694

695 In order to be maximally sensitive to outliers in relative cerebellar volumes, we replaced eTIV with
696 total cerebellar volume in the GAM models of cerebellar regions of interest (i.e., SUIT atlas regions),
697 using the following formula:

698

```
699     GAM_model<-gam(Anatomical feature ~ s(Age, bs = "cs", by = Sex, k = 10) + as.factor(Sex)
700     + as.factor(Scanner) + total cerebellar volume, data = UKBB_cerebellum_GWAS, select =
701     TRUE, method = "REML")
```

702

703 Adjusted cerebral and cerebellar indices were then created by reconstructing the data using the
704 intercept and residuals from these models (i.e., removing estimated effects of age, sex and eTIV or
705 total cerebellar volume), before rejecting 1792 participants with potential outlier cerebral indices and
706 2222 participants with potential outlier cerebellar indices (MAD > +/- 3).

707

708 This iterative QC procedure resulted in the rejection of 5,105 (i.e., 15.3%) of the original 33,317
709 datasets, leaving 28,212 datasets for further analysis.

710

711 **Non-negative matrix factorization**

712 Cerebellar grey matter maps from 28,212 subjects passing the iterative QC procedure were
713 smoothed with a 4mm full-width-half-maximum gaussian kernel in SPM12(76), concatenated across
714 all subjects and multiplied with a binary mask to isolate voxels located in the cerebellar cortex. This
715 cerebellar cortical mask was constructed by multiplying a binary mask containing all 28 cerebellar
716 lobules of the SUIT-atlas with the thresholded (at a value of 0.1) mean (unsmoothed) grey matter
717 segmentation across all 28,212 participants.

718 The smoothed, concatenated and masked grey matter maps were then subjected to
719 orthogonal projective non-negative matrix-factorization (OPNMF)(26), in order to derive data-driven
720 parcellations of regional cerebellar grey matter volume.

721 Non-negative matrix factorization (NNMF) is a blind source separation technique that allows
722 structural brain networks to be described in a hypothesis-free, data-driven way by identifying patterns
723 of covariation in the data. In contrast to alternative techniques, such as principal component analysis
724 and independent component analysis, which yield components with both positive and negative
725 weights that are often difficult to interpret, NNMF produces a sparse, positive-only, parts-based
726 representation of the data. Importantly, NNMF has previously been proven effective in estimating
727 covariance patterns in neuroimaging data while providing an easier interpretation of the results than
728 other matrix decomposition techniques such as principal component analysis (PCA) or independent
729 component analysis (ICA)(26-28, 77, 78).

730 Briefly, NNMF decomposes an input matrix (voxels×subjects) into two matrices; a component
731 matrix W (voxels×k) and a weight matrix H (k×subjects) where k is the number of components that
732 needs to be specified by the user. Here, we used an implementation of orthogonal projective non-
733 negative matrix factorization previously used in a number of publications(26-28, 77, 78) and
734 downloaded from <https://github.com/asotiras/brainparts>. Given the large number of participants, we
735 used the `opnmf_mem.m` function, which has been optimized for high-dimensional data. The function

736 was run with default parameter settings, except for maximal number of iterations, which was increased
737 to 200k, in order to ensure full convergence across all tested model orders.

738

739 **Model order selection**

740 Since the resulting parcellations are highly dependent on the requested number of components (or
741 model order) specified, we tested model orders ranging from 2 to 30 in steps of 1, as well as from
742 30 to 100 in steps of 10. Binarized winner-takes-all (i.e. assigning each voxel to the NNMF
743 component with the highest loading) maps of the resulting decompositions projected onto a flattened
744 representation of the cerebellar cortex are shown in Supplementary Figure 1.

745 Resulting NNMF decompositions were then evaluated based on two criteria; 1) how much of the
746 variance in the original input data a given NNMF solution (i.e., component maps and subject weights)
747 could explain and on 2) how reproducible the component maps were. As a metric of change in
748 explained variance we used the change of the Frobenius norm of the reconstruction error. With
749 increasing model orders the variance explained will always increase and the reconstruction error
750 decrease, but if the decrease in the reconstruction error (or gradient) levels off, this indicates that
751 the intrinsic dimensionality of the data might have been approximated (and that the subsequent
752 increase in explained variance can largely be attributed to fitting random noise in the input data). In
753 order to assess reproducibility, we split the full dataset into two equal sets (matched with respect to
754 scanner site, $n = 14,105$ and $14,107$, respectively), and ran NNMF on each split-half sample. For
755 each set of independent NNMF parcellations, we computed two reproducibility indices. First, for each
756 model order we matched components across split-half runs using the Hungarian algorithm(79),
757 before computing the spatial correlations between matched component maps, and extracting the
758 median correlation across all matched components as our first reproducibility index. For our second
759 reproducibility index, we first computed one overall – and categorical – component map using a
760 “winner-takes-all”-approach, i.e., assigning each voxel to the NNMF component with the highest
761 loading. Next, we calculated the adjusted Rand index (ranging from 0 to 1, with higher values
762 indicating greater similarity(80), across the two categorical parcellation maps for each model order
763 as our second metric of reproducibility.

764 As can be seen in Supplementary Figure 2A, for lower model orders, increasing the model
765 order resulted in a sharp decrease in the reconstruction error, indicating that models with more
766 components resulted in a significantly better fit to the data. However, after reaching model orders
767 between 15 and 30, the incremental improvement in fit from adding another component appeared to
768 level off. As expected, the reproducibility results showed a largely inverse pattern, with both
769 reproducibility indices decreasing with increasing model orders (Supplementary Figure 2B). Of note,
770 for model orders up to 8, median spatial correlations across all matched components was above .99,
771 indicating almost identical parcellations derived from the two independent samples. However, even
772 for a model order of 100, the median pairwise correlation was still pretty high (.85), with 60% of
773 components showing pairwise spatial correlations above 0.8, suggesting a reasonable level of

774 reproducibility even for the most fine-grained parcellation. Our reproducibility index for the
775 categorical parcellations showed very similar results; the adjusted Rand index remained above .9
776 for model orders up to 8, and then decreased to 0.56 at a model order of 100.

777 Given that the change in reconstruction error appeared to stabilize between 15 and 30
778 components, indicating that the intrinsic dimensionality of the data had been approximated, we
779 searched for the most reproducible parcellations within this range. Since the reliability estimates for
780 model orders of 16 and 23 were very similar, with the 23-component solution explaining more of the
781 variance in the original data, we used the 23-component parcellation for all further analyses.

782

783 **Adjustment and rank-order normalization of anatomical indices**

784 Prior to being subjected to genome-wide association analyses, we adjusted all anatomical indices
785 for effects of age, sex, estimated total intracranial volume, scanner site, 40 genetic population
786 components, genetic batch and mean Euler number (i.e, an index of MRI image quality(29),
787 averaged across hemispheres). Finally, all adjusted anatomical indices were inverse rank
788 normalized(81).

789

790 **Pre-processing of genetic data**

791 For all genetic analyses we made use of the UKB v3 imputed data, which has undergone extensive
792 quality control procedures as described by the UKB genetics team(82). After converting the BGEN
793 format to PLINK binary format, we additionally carried out standard quality check procedures. We
794 first selected White Europeans, as determined by a combination of self-identification as 'White
795 British' and similar genetic ancestry based on genetic principal components, that had undergone the
796 neuroimaging protocol. We then filtered out individuals with more than 10% missingness, removed
797 SNPs with low imputation quality scores ($INFO < .5$), SNPs with more than 10% missingness, and
798 SNPs failing the Hardy-Weinberg equilibrium test at $p=1*10^{-9}$. We further set a minor allele
799 frequency threshold of 0.005 leaving 9,061,238 SNPs. After estimating the genetic relationship
800 matrix (GRM) using genetic complex trait analysis (GCTA(31)), we finally removed 910 participants
801 defined as close relatives using a threshold of 0.05 (approximately corresponding to 3rd cousins).

802

803 **Heritability estimation and genetic correlation analyses**

804 SNP-based heritability estimates for all morphological features – as well as the pairwise genetic
805 correlations between cerebellar features - were estimated using genetic complex trait analysis
806 (GCTA(31)).

807

808 **Univariate genome-wide association analyses**

809 Univariate analyses of total cerebellar grey matter volume and the ten cerebral comparison
810 phenotypes were conducted using Plink v1.9.

811

812 **Genetic correlation analyses across discovery and replication samples and with previous**
813 **published GWASs**

814 Genetic correlation analyses across different samples were conducted using LD-score
815 regression(30).

816

817 **Multivariate genome-wide association analyses**

818 For our main analysis, we used a recently developed multivariate analysis method (MOSTest(34)),
819 to conduct a multivariate genome-wide association (GWA) analysis on cerebellar morphological
820 features. MOSTest identifies genetic effects across multiple phenotypes, yielding a multivariate
821 GWAS summary statistic across all 23 features, and provides robust (permutation based) test
822 statistics. For mathematical details of the implementation, see van der Meer et al. (2020)(34), for
823 details on the software implementation see github.com/precimed/mostest. MOSTest has been
824 extensively validated in the original methods paper, including simulations and comparisons with
825 other methods that have confirmed its solid discovery performance as well as an order of magnitude
826 shorter runtime compared to other tools(34). For comparison to standard univariate approaches, we
827 also performed univariate GWASs (extracted from the univariate stream of MOSTest(34) and
828 identical to results from analyses using Plink).

829

830 **Multivariate replication analysis**

831 To ensure that not only single lead SNP associations replicate but that also the multivariate pattern
832 of these associations are consistent in the discovery and replication sample, we implemented a
833 multivariate replication procedure established in Loughnan et al.(37). In brief, for each lead SNP
834 identified in the multivariate analysis in the discovery sample, this procedure derives a composite
835 score from the mass-univariate z-statistics and tests for associations of the composite score with the
836 genotype in the replication sample (for mathematical formulation see Loughnan et al.(37)). 19 of the
837 560 lead SNPs could not be tested as they were not available in the replication sample. For the
838 remaining SNPs we report the percent of loci replicating at $P < 0.05$, the percent remaining significant
839 after Bonferroni correction for 541 conducted tests, and the percent of lead SNPs showing the same
840 effect direction. In addition, we report the percentage of genetic loci replicated (defined as containing
841 at least one replicating lead SNP).

842

843 **Multivariate cerebral comparison phenotypes**

844 To compare key multivariate cerebellar results with other multivariate brain phenotypes, we
845 downloaded summary statistics from two recent studies on cerebrocortical(42) and hippocampal(43)
846 regional morphology. These comparison summary statistics were next analyzed using FUMA(35) as
847 described for the main cerebellar results below.

848

849 **Locus identification and SNP annotation**

850 To identify genetic loci we uploaded summary statistics to the FUMA platform v1.4.1(35) Using the
851 1000GPhase3 EUR as reference panel, we identified independent SNPs as SNPs below the
852 significance threshold of $P < 5e-8$ that were also in linkage equilibrium with each other at $r^2 < 0.6$.
853 For each independent SNP, all candidate variants are identified as variants with LD $r^2 \geq 0.6$ with the
854 independent SNP. A fraction of the independent significant SNPs in approximate linkage equilibrium
855 with each other at $r^2 < 0.1$ were considered as lead SNPs. For a given lead SNP, the borders of the
856 genomic locus are defined as min/max positional coordinates over all corresponding candidate
857 SNPs. Finally, loci are merged if they are separated by less than 250kb.

858 FUMA further annotates associated SNPs based on functional categories, Combined
859 Annotation Dependent Depletion (CADD) scores which predicts the deleteriousness of SNPs on
860 protein structure/function(54), RegulomeDB scores which predicts regulatory functions(83); and
861 chromatin states that shows the transcription/regulation effects of chromatin states at the SNP
862 locus(84). For all these analyses, we used default FUMA parameters.

863

864 **Genome-wide gene-based association and gene-set analyses**

865 We conducted genome-wide gene-based association and gene-set analyses using MAGMA
866 v.1.10(49) (<http://ctg.cncr.nl/software/magma>). MAGMA performs multiple linear regression to map
867 the input SNPs to 19,190 protein coding genes and estimates the significance value of that gene.
868 Genes were considered significant if the P value was < 0.05 after Bonferroni correction for 19,190
869 genes. The same procedure was used for MAGMA analysis of summary statistics for the three
870 multivariate cerebral comparison phenotypes (cerebrocortical thickness and surface area(42) and
871 regional hippocampal volumes(43)).

872 MAGMA gene-level statistics were next used as input to gene-property and gene-set
873 analyses in MAGMA. Gene-property analyses test for associations between tissue specific gene
874 expression profiles and disease-gene associations. The gene-property analysis is based on the
875 regression model: $Z \sim \beta_0 + E_t \beta_E + A \beta_A + B \beta_B + \epsilon$, where Z is a gene-based Z-score converted from
876 the gene-based P-value, B is a matrix of several technical confounders included by default (e.g.,
877 gene size, gene density, sample size), E_t is the gene expression value of a testing tissue type and A
878 is the average expression across all tissue types in a data set (ensuring a test of expression
879 specificity). We performed a one-sided test ($\beta_E > 0$) which is essentially testing the positive
880 relationship between tissue specificity and genetic association of genes.

881 We tested associations with two regional brain gene expression datasets (Allen Human
882 Brain Atlas(33) and GTEx) and one developmental brain gene expression dataset (BrainSpan). For
883 extraction and processing of gene expression data, see below.

884

885 **Extraction and processing of gene expression data**

886 *Allen Human Brain Atlas*: Regional microarray expression data were obtained from 6 post-mortem
887 brains (1 female, ages 24.0--57.0, 42.50 +/- 13.38) provided by the Allen Human Brain Atlas(33).

888 Data were processed with the abagen toolbox (version 0.1.3) (32) using two volumetric atlases; 1)
889 the binarized 23-region NNMF-derived parcellation of the cerebellar cortex; and 2) a modified version
890 of the Desikan atlas where ROIs were merged to construct 9 bilateral regions: cerebellum, cerebral
891 cortex, pallidum, caudate, putamen, thalamus, amygdala, nucleus accumbens and hippocampus.

892 First, microarray probes were reannotated using data provided by Arnatkeviciute, Fulcher
893 and Fornito(85); probes not matched to a valid Entrez ID were discarded. Next, probes were filtered
894 based on their expression intensity relative to background noise(86), such that probes with intensity
895 less than the background in $\geq 50.00\%$ of samples across donors were discarded, yielding 31,569
896 probes. When multiple probes indexed the expression of the same gene, we selected and used the
897 probe with the most consistent pattern of regional variation across donors (i.e., differential
898 stability(87)), calculated with:

$$\Delta_S(p) = \frac{1}{\binom{N}{2}} \sum_{i=1}^{N-1} \sum_{j=i+1}^N \rho[B_i(p), B_j(p)]$$

899
900 where ρ is Spearman's rank correlation of the expression of a single probe, p , across regions
901 in two donors B_i and B_j , and N is the total number of donors.

902 Here, regions correspond to the structural designations provided in the ontology from the
903 AHBA. The MNI coordinates of tissue samples were updated to those generated via non-linear
904 registration using the Advanced Normalization Tools (ANTs; <https://github.com/chrisfilo/alleninf>).
905 Samples were assigned to brain regions in the provided atlas if their MNI coordinates were within 2
906 mm of a given parcel. To reduce the potential for misassignment, sample-to-region matching was
907 constrained by hemisphere and gross structural divisions (i.e., cortex, subcortex/ brainstem, and
908 cerebellum, such that e.g., a sample in the left cortex could only be assigned to an atlas parcel in
909 the left cortex(85)). All tissue samples not assigned to a brain region in the provided atlas were
910 discarded. \n\nInter-subject variation was addressed by normalizing tissue sample expression
911 values across genes using a robust sigmoid function(88):

$$x_{norm} = \frac{1}{1 + \exp\left(-\frac{(x - \langle x \rangle)}{IQR_x}\right)}$$

912
913 where $\langle x \rangle$ is the median and IQR_x is the normalized interquartile range of the expression of a
914 single tissue sample across genes. Normalized expression values were then rescaled to the unit
915 interval:

$$x_{scaled} = \frac{x_{norm} - \min(x_{norm})}{\max(x_{norm}) - \min(x_{norm})}$$

916
917 Gene expression values were then normalized across tissue samples using an identical
918 procedure. Samples assigned to the same brain region were averaged separately for each donor

919 and then across donors, yielding two regional expression matrices with 23 and 9 rows, corresponding
920 to brain regions, and 15,631 and 15,633 columns, corresponding to the retained genes. Prior to
921 inclusion in MAGMA gene property analyses, we converted gene names for the modified Desikan
922 atlas to ENSEMBL IDs, and calculated the mean expression value across tissue types (in order to
923 include this as a covariate in MAGMA analyses testing for gene expression specificity), resulting in
924 a 10 (regions) by (15,490) gene expression matrix.

925

926 *GTeX*: Text files containing median transcript per millimeter (TPM) values for 53 tissue types
927 (*GTEX_Analysis_2017-06-05_v8_RNASeqCv1.1.9_gene_median_tpm.gct.gz*) were down-loaded
928 from the *GTEX* portal (<https://gtexportal.org/home/datasets/>). After selecting only expression data
929 from the seven (out of nine) comparison brain regions present in the *GTEX* dataset (i.e., amygdala,
930 caudate, cerebellum, cortex, hippocampus, nucleus accumbens and putamen), we filtered the data
931 by only including genes with median TPM values above 1 for at least one of these tissue type
932 (retaining 19,578 of 56,200 annotated genes). Following the procedure used by FUMA(35), we next
933 winsorized median TPM values at 50 (i.e., replaced $TPM > 50$ with 50), before log transforming TPM
934 with pseudocount 1 ($\log_2(RPKM+1)$). Finally, we calculated the mean expression value across tissue
935 types (in order to include this as a covariate in MAGMA analyses testing for gene expression
936 specificity).

937

938 *BrainSpan data*: The analysis of *BrainSpan* data testing for developmentally specific brain
939 expression was performed entirely within FUMA v1.4.1., using default parameters.

940

941 **Analysis of Human Dating Genome Data.** The Atlas of Variant Age for chromosomes 1-22 was
942 downloaded from the Human Genome Dating (HGD) website: <https://human.genome.dating/>. This
943 atlas contains more than 45 million SNPs which has been assigned dates of origin based on a
944 recombination clock and mutation clock applied to two large-scale sequencing datasets (1000
945 Genomes Project(89) and The Simons Genome Diversity Project(90)), with no assumptions made
946 about demographic or selective processes(44). The current study used the median joint age
947 estimates from both clocks when analyzing SNPs present in both datasets in combination (i.e.,
948 13,694,493 SNPs).

949 After merging dated SNPs with the 40,405,505 SNPs also present in the Haplotype
950 Reference Consortium reference data (to add minor allele frequencies, MAF) and removing 715,083
951 (5.2%) SNPs with missing MAF values as well as the very few (14,549, 0.1%) SNPs dated older
952 than 2 million years, 12,960,066 SNPs remained. 146,977 of these dated SNPs were matched to
953 candidate SNPs linked to cerebellar morphology or any of the comparison brain phenotypes,
954 hereafter referred to as brain-SNPs. Partially because very rare variants (Minor Allele
955 Frequency/MAF < 0.005) had been removed prior to the multivariate GWAS analysis, MAF was not
956 equally distributed between these brain-SNPs and the full range of dated SNPs in the HGD dataset.

957 Importantly, MAF has been shown to be systematically related to the estimated age of SNPs, with a
958 higher proportion of low-MAF SNPs in more recent than in older time-bins(44, 45). Consequently,
959 following the analysis approach established by Libedinsky et al. (45), we first determined the MAF-
960 distribution of brain-SNPs (across eight bins: <0.0001; 0.0001-0.001; 0.001-0.01; 0.01-0.1; 0.1-0.2;
961 0.2-0.3; 0.3-0.4; 0.4-0.5) and selected random set of 2,645,586 SNPs from the HGD dataset that
962 were matched to the brain-SNPs in terms of MAF-bin distribution.

963 For statistical inference we constructed null models (separate for each brain phenotype) by
964 randomly drawing sets of SNPs (of equal size to the number of phenotype-linked candidate SNPs)
965 from the MAF-matched HGD-dataset and computing the histograms of estimated dates from 0 to 2
966 million years ago (divided into 100 bins of 20,000 years) over 10,000 iterations. From these null
967 models we extracted bin means and standard deviations (used to assign z-scores to the bin values
968 of brain phenotype histograms), as well as significance thresholds (defined as the upper and lower
969 99.95th percentile of the null model (i.e. corresponding to a Bonferroni corrected threshold of 0.05
970 across 100 bins).

971

972 **Positional and eQTL mapping of SNPs to plausible causal genes**

973 In addition to using MAGMA, we also mapped candidate SNPs to plausible causal genes using two
974 complementary gene mapping strategies implemented in FUMA(35): 1) Positional mapping of
975 deleterious SNPs (defined as having a CADD-score > 12.37) and 2) eQTL-mapping of SNPs
976 previously shown to alter gene expression in cerebellar tissue (from the BRAINEAC and GTEx v8
977 databases). These analyses were run with default FUMA parameters. For the three multivariate
978 cerebral comparison phenotypes (i.e., cerebrocortical thickness, cerebrocortical surface area and
979 hippocampal regional volumes), we employed identical gene mapping procedures to our cerebellar
980 morphology results, except for the tissues chosen for eQTL mapping (cerebrocortical and
981 hippocampal, respectively).

982

983 **Gene set analyses using lists of mapped genes**

984 All gene set analyses using mapped genes were conducted using the hypeR R-package (91). This
985 package implements the hypergeometric test (also known as Fisher's exact test), which assigns a
986 p-value to gene-set overlaps given gene set sizes and the number of background genes. This R-
987 package also contains functions for downloading and/or formatting gene sets. The following gene
988 sets were accessed using hypeR: "Allen_Brain_Atlas_up" (regional overexpression in the Allen
989 Muse Brain Atlas), "MGI_Mammalian_PhenoType_Level_4_2021", "DisGeNet" (all from the enrichR
990 platform. In addition, we downloaded sets of genes with regional overexpression in the Allen Human
991 Brain Atlas from the Harmonizome platform(92) and accessed a list of genes mapped to human
992 accelerated regions(93). For all gene-set analyses we employed Bonferroni-correction by dividing
993 the p-value threshold of 0.05 by the number of gene sets included in each analysis.

994

995 **Genetic overlap between cerebellar morphology and brain disorders**

996 We accessed GWAS summary statistics for attention deficit hyperactivity disorder (ADHD)(94),
997 autism spectrum disorder (ASD)(95), bipolar disorder (BIP)(96) and major depressive disorder
998 (MDD)(97) from the Psychiatric Genomics Consortium. In order to avoid sample overlap, for MDD
999 we used summary statistics based on a sample with the UK Biobank participants removed. 23&me
000 participants included in the original MDDGWAS were also excluded, since these data are not freely
001 available). Finally, we included data from a recent study of schizophrenia (SCZ)(98). Shared variants
002 associated with cerebellar morphology and each of the above-mentioned brain disorders were
003 identified using conjunctive FDR statistics ($FDR < 0.05$)(99, 100). In contrast to genetic correlation
004 analysis, conjunctive FDR does not require effect directions and can therefore be applied to
005 summary statistics from multivariate GWAS, which do not contain effect directions. Two genomic
006 regions, the extended major histocompatibility complex genes region (hg19 location Chr 6:
007 25119106–33854733) and chromosome 8p23.1 (hg19 location Chr 8: 7242715–12483982) for all
008 cases and *APOE* region for ASD, were excluded from the FDR-fitting procedures because complex
009 correlations in regions with intricate LD can bias FDR estimation. We submitted the results from
010 conjunctive FDR to FUMA v1.3.7(35) to annotate the genomic loci with conjFDR value < 0.10
011 having an $r^2 \geq 0.6$ with one of the independent significant lead SNPs. Genetic correlations between
012 univariate results for the 23 cerebellar features, the 10 comparison brain phenotypes, and each of
013 the five mental disorders were computed using LD-score regression as described above.

014

References for Online Methods:

1. S. Herculano-Houzel, *The human advantage : a new understanding of how our brain became remarkable* (The MIT Press, Cambridge, Massachusetts, 2016), pp. xiii, 256 pages.
2. R. A. Barton, C. Venditti, in *Curr. Biol.* (2014).
3. M. I. Sereno, J. Diedrichsen, M. Tachrount, G. Testa-Silva, H. d'Arceuil, C. De Zeeuw, The human cerebellum has almost 80% of the surface area of the neocortex. *Proc Natl Acad Sci U S A* **117**, 19538-19543 (2020).
4. P. W. Harrison, S. H. Montgomery, Genetics of Cerebellar and Neocortical Expansion in Anthropoid Primates: A Comparative Approach. *Brain Behav Evol* **89**, 274-285 (2017).
5. H. C. Leiner, A. L. Leiner, R. S. Dow, in *Trends in Neurosciences*. (1993), vol. 16, pp. 444-447.
6. P. L. Strick, R. P. Dum, J. A. Fiez, in *Annu. Rev. Neurosci.* (2009), vol. 32, pp. 413-434.
7. R. L. Buckner, in *Neuron*. (2013), vol. 80, pp. 807-815.
8. M. King, C. R. Hernandez-Castillo, R. A. Poldrack, R. B. Ivry, J. Diedrichsen, Functional boundaries in the human cerebellum revealed by a multi-domain task battery. *Nat Neurosci* **22**, 1371-1378 (2019).
9. S. S. Wang, A. D. Kloth, A. Badura, The cerebellum, sensitive periods, and autism. *Neuron* **83**, 518-532 (2014).
10. T. Moberget, N. T. Doan, D. Alnaes, T. Kaufmann, A. Cordova-Palomera, T. V. Lagerberg, J. Diedrichsen, E. Schwarz, M. Zink, S. Eisenacher, P. Kirsch, E. G. Jonsson, H. Fatouros-Bergman, L. Flyckt, KaSp, G. Pergola, T. Quarto, A. Bertolino, D. Barch, A. Meyer-Lindenberg, I. Agartz, O. A. Andreassen, L. T. Westlye, Cerebellar volume and cerebellocerebral structural covariance in schizophrenia: a multisite mega-analysis of 983 patients and 1349 healthy controls. *Mol Psychiatry* **23**, 1512-1520 (2018).
11. H. H. Adams, D. P. Hibar, V. Chouraki, J. L. Stein, P. A. Nyquist, M. E. Renteria, S. Trompet, A. Arias-Vasquez, S. Seshadri, S. Desrivieres, A. H. Beecham, N. Jahanshad, K. Wittfeld, S. J. Van der Lee, L. Abramovic, S. Alhusaini, N. Amin, M. Andersson, K. Arfanakis, B. S. Aribisala, N. J. Armstrong, L. Athanasiu, T. Axelsson, A. Beiser, M. Bernard, J. C. Bis, L. M. Blanken, S. H. Blanton, M. M. Bohlken, M. P. Boks, J. Bralten, A. M. Brickman, O. Carmichael, M. M. Chakravarty, G. Chauhan, Q. Chen, C. R. Ching, G. Cuellar-Partida, A. D. Braber, N. T. Doan, S. Ehrlich, I. Filippi, T. Ge, S. Giddaluru, A. L. Goldman, R. F. Gottesman, C. U. Greven, O. Grimm, M. E. Griswold, T. Guadalupe, J. Hass, U. K. Haukvik, S. Hilal, E. Hofer, D. Hoehn, A. J. Holmes, M. Hoogman, D. Janowitz, T. Jia, D. Kasperaviciute, S. Kim, M. Klein, B. Kraemer, P. H. Lee, J. Liao, D. C. Liewald, L. M. Lopez, M. Luciano, C. Macare, A. Marquand, M. Matarin, K. A. Mather, M. Mattheisen, B. Mazoyer, D. R. McKay, R. McWhirter, Y. Milaneschi, N. Mirza-Schreiber, R. L. Muetzel, S. M. Maniega, K. Nho, A. C. Nugent, L. M. Loohuis, J. Oosterlaan, M. Pampmeyer, I. Pappa, L. Pirpamer, S. Pudas, B. Putz, K. B. Rajan, A. Ramasamy, J. S. Richards, S. L. Risacher, R. Roiz-Santianez, N. Rommelse, E. J. Rose, N. A. Royle, T. Rundek, P. G. Samann, C. L. Satizabal, L. Schmaal, A. J. Schork, L. Shen, J. Shin, E. Shumskaya, A. V. Smith, E. Sprooten, L. T. Strike, A. Teumer, R. Thomson, D. Tordesillas-Gutierrez, R. Toro, D. Trabzuni, D. Vaidya, J. Van der Grond, D. Van der Meer, M. M. Van Donkelaar, K. R. Van Eijk, T. G. Van Erp, D. Van Rooij, E. Walton, L. T. Westlye, C. D. Whelan, B. G. Windham, A. M. Winkler, G. Woldehawariat, C. Wolf, T. Wolfers, B. Xu, L. R. Yanek, J. Yang, A. Zijdenbos, M. P. Zwiers, I. Agartz, N. T. Aggarwal, L. Almasy, D. Ames, P. Amouyel, O. A. Andreassen, S. Arepalli, A. A. Assareh, S. Barral, M. E. Bastin, D. M. Becker, J. T. Becker, D. A. Bennett, J. Blangero, H. van Bokhoven, D. I. Boomsma, H. Brodaty, R. M. Brouwer, H. G. Brunner, R. L. Buckner, J. K. Buitelaar, K. B. Bulayeva, W. Cahn, V. D. Calhoun, D. M. Cannon, G. L. Cavalleri, C. Chen, C. Y. Cheng, S. Cichon, M. R. Cookson, A. Corvin, B. Crespo-Facorro, J. E. Curran, M. Czisch, A. M. Dale, G. E. Davies, E. J. De Geus, P. L. De Jager, G. I. de Zubicaray, N. Delanty, C. Depondt, A. L. DeStefano, A. Dillman, S. Djurovic, G. Donohoe, W. C. Drevets, R. Duggirala, T. D. Dyer, S. Erk, T. Espeseth, D. A. Evans, I. O. Fedko, G. Fernandez, L. Ferrucci, S. E. Fisher, D. A. Fleischman, I. Ford, T. M. Foroud, P. T. Fox, C. Francks, M. Fukunaga, J. R. Gibbs, D. C. Glahn, R. L. Gollub, H. H. Goring, H. J. Grabe, R. C. Green, O. Gruber, V. Gudnason, S. Guelfi, N. K.

Hansell, J. Hardy, C. A. Hartman, R. Hashimoto, K. Hegenscheid, A. Heinz, S. Le Hellard, D. G. Hernandez, D. J. Heslenfeld, B. C. Ho, P. J. Hoekstra, W. Hoffmann, A. Hofman, F. Holsboer, G. Homuth, N. Hosten, J. J. Hottenga, H. E. Pol, M. Ikeda, M. K. Ikram, C. R. Jack, Jr., M. Jenkinson, R. Johnson, E. G. Jonsson, J. W. Jukema, R. S. Kahn, R. Kanai, I. Kloszewska, D. S. Knopman, P. Kochunov, J. B. Kwok, S. M. Lawrie, H. Lemaitre, X. Liu, D. L. Longo, W. T. Longstreth, Jr., O. L. Lopez, S. Lovestone, O. Martinez, J. L. Martinot, V. S. Mattay, C. McDonald, A. M. McIntosh, K. L. McMahon, F. J. McMahon, P. Mecocci, I. Melle, A. Meyer-Lindenberg, S. Mohnke, G. W. Montgomery, D. W. Morris, T. H. Mosley, T. W. Muhleisen, B. Muller-Myhsok, M. A. Nalls, M. Nauck, T. E. Nichols, W. J. Niessen, M. M. Nothen, L. Nyberg, K. Ohi, R. L. Olvera, R. A. Ophoff, M. Pandolfo, T. Paus, Z. Pausova, B. W. Penninx, G. B. Pike, S. G. Potkin, B. M. Psaty, S. Reppermund, M. Rietschel, J. L. Roffman, N. Romanczuk-Seiferth, J. I. Rotter, M. Ryten, R. L. Sacco, P. S. Sachdev, A. J. Saykin, R. Schmidt, P. R. Schofield, S. Sigurdsson, A. Simmons, A. Singleton, S. M. Sisodiya, C. Smith, J. W. Smoller, H. Soininen, V. Srikanth, V. M. Steen, D. J. Stott, J. E. Sussmann, A. Thalamuthu, H. Tiemeier, A. W. Toga, B. J. Traynor, J. Troncoso, J. A. Turner, C. Tzourio, A. G. Uitterlinden, M. C. Hernandez, M. Van der Brug, A. Van der Lugt, N. J. Van der Wee, C. M. Van Duijn, N. E. Van Haren, T. E. D. Van, M. J. Van Tol, B. N. Vardarajan, D. J. Veltman, M. W. Vernooij, H. Volzke, H. Walter, J. M. Wardlaw, T. H. Wassink, M. E. Weale, D. R. Weinberger, M. W. Weiner, W. Wen, E. Westman, T. White, T. Y. Wong, C. B. Wright, H. R. Zielke, A. B. Zonderman, I. J. Deary, C. DeCarli, H. Schmidt, N. G. Martin, A. J. De Craen, M. J. Wright, L. J. Launer, G. Schumann, M. Fornage, B. Franke, S. Dobbie, S. E. Medland, M. A. Ikram, P. M. Thompson, Novel genetic loci underlying human intracranial volume identified through genome-wide association. *Nat Neurosci* **19**, 1569-1582 (2016).

12. D. van der Meer, J. Rokicki, T. Kaufmann, A. Cordova-Palomera, T. Moberget, D. Alnaes, F. Bettella, O. Frei, N. T. Doan, I. E. Sonderby, O. B. Smeland, I. Agartz, A. Bertolino, J. Bralten, C. L. Brandt, J. K. Buitelaar, S. Djurovic, M. van Donkelaar, E. S. Dorum, T. Espeseth, S. V. Faraone, G. Fernandez, S. E. Fisher, B. Franke, B. Haatveit, C. A. Hartman, P. J. Hoekstra, A. K. Haberg, E. G. Jonsson, K. K. Kolskar, S. Le Hellard, M. J. Lund, A. J. Lundervold, A. Lundervold, I. Melle, J. Monereo Sanchez, L. C. Norbom, J. E. Nordvik, L. Nyberg, J. Oosterlaan, M. Papalino, A. Papassotiropoulos, G. Pergola, D. J. F. de Quervain, G. Richard, A. M. Sanders, P. Selvaggi, E. Shumskaya, V. M. Steen, S. Tonnesen, K. M. Ulrichsen, M. P. Zwiers, O. A. Andreassen, L. T. Westlye, I. Alzheimer's Disease Neuroimaging, N. Pediatric Imaging, S. Genetics, Brain scans from 21,297 individuals reveal the genetic architecture of hippocampal subfield volumes. *Mol Psychiatry*, (2018).

13. T. Chambers, V. Escott-Price, S. Legge, E. Baker, K. D. Singh, J. T. R. Walters, X. Caseras, R. J. L. Anney, Genetic common variants associated with cerebellar volume and their overlap with mental disorders: a study on 33,265 individuals from the UK-Biobank. *Mol Psychiatry* **27**, 2282-2290 (2022).

14. E. Tissink, S. C. de Lange, J. E. Savage, D. P. Wightman, C. A. de Leeuw, K. M. Kelly, M. Nagel, M. P. van den Heuvel, D. Posthuma, Genome-wide association study of cerebellar volume provides insights into heritable mechanisms underlying brain development and mental health. *Commun Biol* **5**, 710 (2022).

15. S. Macri, Y. Savriama, I. Khan, N. Di-Poi, Comparative analysis of squamate brains unveils multi-level variation in cerebellar architecture associated with locomotor specialization. *Nat Commun* **10**, 5560 (2019).

16. J. B. Smaers, A. H. Turner, A. Gomez-Robles, C. C. Sherwood, A cerebellar substrate for cognition evolved multiple times independently in mammals. *Elife* **7**, (2018).

17. K.-H. E, S.-H. A. Chen, M.-H. R. Ho, J. E. Desmond, in *Hum Brain Mapp.* (2014), vol. 35, pp. 593-615.

18. C. J. Stoodley, J. D. Schmahmann, in *NeuroImage.* (2009), vol. 44, pp. 489-501.

19. R. L. Buckner, F. M. Krienen, A. Castellanos, J. C. Diaz, B. T. T. Yeo, in *Journal of Neurophysiology.* (2011), vol. 106, pp. 2322-2345.

- 120 20. L. Sang, W. Qin, Y. Liu, W. Han, Y. Zhang, T. Jiang, C. Yu, in *NeuroImage*. (Elsevier Inc., 2012),
121 vol. 61, pp. 1213-1225.
- 122 21. F. M. Krienen, R. L. Buckner, in *Cerebral Cortex*. (2009), vol. 19, pp. 2485-2497.
- 123 22. J. A. Bernard, R. D. Seidler, K. M. Hassevoort, B. L. Benson, R. C. Welsh, J. L. Wiggins, S. M.
124 Jaeggi, M. Buschkuhl, C. S. Monk, J. Jonides, S. J. Peltier, in *Front Neuroanat*. (2012), vol. 6,
125 pp. 31.
- 126 23. J. A. Kipping, W. Grodd, V. Kumar, M. Taubert, A. Villringer, D. S. Margulies, in *NeuroImage*.
127 (2013), vol. 83, pp. 837-848.
- 128 24. C. Wang, J. Kipping, C. Bao, H. Ji, A. Qiu, Cerebellar Functional Parcellation Using Sparse
129 Dictionary Learning Clustering. *Front Neurosci* **10**, 188 (2016).
- 130 25. J. A. Kipping, T. A. Tuan, M. V. Fortier, A. Qiu, Asynchronous Development of Cerebellar,
131 Cerebello-Cortical, and Cortico-Cortical Functional Networks in Infancy, Childhood, and
132 Adulthood. *Cereb Cortex*, (2016).
- 133 26. A. Sotiras, S. M. Resnick, C. Davatzikos, Finding imaging patterns of structural covariance via
134 Non-Negative Matrix Factorization. *Neuroimage* **108**, 1-16 (2015).
- 135 27. A. Sotiras, J. B. Toledo, R. E. Gur, R. C. Gur, T. D. Satterthwaite, C. Davatzikos, Patterns of
136 coordinated cortical remodeling during adolescence and their associations with functional
137 specialization and evolutionary expansion. *Proc Natl Acad Sci U S A* **114**, 3527-3532 (2017).
- 138 28. D. P. Varikuti, S. Genon, A. Sotiras, H. Schwender, F. Hoffstaedter, K. R. Patil, C. Jockwitz, S.
139 Caspers, S. Moebus, K. Amunts, C. Davatzikos, S. B. Eickhoff, Evaluation of non-negative matrix
140 factorization of grey matter in age prediction. *Neuroimage* **173**, 394-410 (2018).
- 141 29. A. F. G. Rosen, D. R. Roalf, K. Ruparel, J. Blake, K. Seelaus, L. P. Villa, R. Ciric, P. A. Cook, C.
142 Davatzikos, M. A. Elliott, A. Garcia de La Garza, E. D. Gennatas, M. Quarmley, J. E. Schmitt, R.
143 T. Shinohara, M. D. Tisdall, R. C. Craddock, R. E. Gur, R. C. Gur, T. D. Satterthwaite,
144 Quantitative assessment of structural image quality. *Neuroimage* **169**, 407-418 (2018).
- 145 30. B. K. Bulik-Sullivan, P. R. Loh, H. K. Finucane, S. Ripke, J. Yang, C. Schizophrenia Working
146 Group of the Psychiatric Genomics, N. Patterson, M. J. Daly, A. L. Price, B. M. Neale, LD Score
147 regression distinguishes confounding from polygenicity in genome-wide association studies. *Nat*
148 *Genet* **47**, 291-295 (2015).
- 149 31. J. Yang, S. H. Lee, M. E. Goddard, P. M. Visscher, GCTA: a tool for genome-wide complex trait
150 analysis. *Am J Hum Genet* **88**, 76-82 (2011).
- 151 32. R. D. Markello, A. Arnatkeviciute, J. B. Poline, B. D. Fulcher, A. Fornito, B. Misic, Standardizing
152 workflows in imaging transcriptomics with the abagen toolbox. *Elife* **10**, (2021).
- 153 33. M. J. Hawrylycz, E. S. Lein, A. L. Guillozet-Bongaarts, E. H. Shen, L. Ng, J. A. Miller, L. N. van
154 de Lagemaat, K. A. Smith, A. Ebbert, Z. L. Riley, C. Abajian, C. F. Beckmann, A. Bernard, D.
155 Bertagnolli, A. F. Boe, P. M. Cartagena, M. M. Chakravarty, M. Chapin, J. Chong, R. A. Dalley,
156 B. David Daly, C. Dang, S. Datta, N. Dee, T. A. Dolbeare, V. Faber, D. Feng, D. R. Fowler, J.
157 Goldy, B. W. Gregor, Z. Haradon, D. R. Haynor, J. G. Hohmann, S. Horvath, R. E. Howard, A.
158 Jeromin, J. M. Jochim, M. Kinnunen, C. Lau, E. T. Lazarz, C. Lee, T. A. Lemon, L. Li, Y. Li, J. A.
159 Morris, C. C. Overly, P. D. Parker, S. E. Parry, M. Reding, J. J. Royall, J. Schulkin, P. A.
160 Sequeira, C. R. Slaughterbeck, S. C. Smith, A. J. Sodt, S. M. Sunkin, B. E. Swanson, M. P.
161 Vawter, D. Williams, P. Wohnoutka, H. R. Zielke, D. H. Geschwind, P. R. Hof, S. M. Smith, C.
162 Koch, S. G. N. Grant, A. R. Jones, An anatomically comprehensive atlas of the adult human
163 brain transcriptome. *Nature* **489**, 391-399 (2012).
- 164 34. D. van der Meer, O. Frei, T. Kaufmann, A. A. Shadrin, A. Devor, O. B. Smeland, W. K. Thompson,
165 C. C. Fan, D. Holland, L. T. Westlye, O. A. Andreassen, A. M. Dale, Understanding the genetic
166 determinants of the brain with MOSTest. *Nat Commun* **11**, 3512 (2020).
- 167 35. K. Watanabe, E. Taskesen, A. van Bochoven, D. Posthuma, Functional mapping and annotation
168 of genetic associations with FUMA. *Nat Commun* **8**, 1826 (2017).
- 169 36. K. Wang, M. Li, H. Hakonarson, ANNOVAR: functional annotation of genetic variants from high-
170 throughput sequencing data. *Nucleic Acids Res* **38**, e164 (2010).
- 171 37. R. J. Loughnan, A. A. Shadrin, O. Frei, D. van der Meer, W. Zhao, C. E. Palmer, W. K.
172 Thompson, C. Makowski, T. L. Jernigan, O. A. Andreassen, C. C. Fan, A. M. Dale,

173 Generalization of cortical MOSTest genome-wide associations within and across samples.
174 *Neuroimage* **263**, 119632 (2022).

- 175 38. S. van der Sluis, D. Posthuma, C. V. Dolan, TATES: efficient multivariate genotype-phenotype
176 analysis for genome-wide association studies. *PLoS Genet* **9**, e1003235 (2013).
- 177 39. P. F. O'Reilly, C. J. Hoggart, Y. Pomyen, F. C. Calboli, P. Elliott, M. R. Jarvelin, L. J. Coin,
178 MultiPhen: joint model of multiple phenotypes can increase discovery in GWAS. *PLoS One* **7**,
179 e34861 (2012).
- 180 40. B. Zhao, T. Luo, T. Li, Y. Li, J. Zhang, Y. Shan, X. Wang, L. Yang, F. Zhou, Z. Zhu, I. Alzheimer's
181 Disease Neuroimaging, N. Pediatric Imaging, Genetics, H. Zhu, Genome-wide association
182 analysis of 19,629 individuals identifies variants influencing regional brain volumes and refines
183 their genetic co-architecture with cognitive and mental health traits. *Nat Genet* **51**, 1637-1644
184 (2019).
- 185 41. S. M. Smith, G. Douaud, W. Chen, T. Hanayik, F. Alfaro-Almagro, K. Sharp, L. T. Elliott, An
186 expanded set of genome-wide association studies of brain imaging phenotypes in UK Biobank.
187 *Nat Neurosci* **24**, 737-745 (2021).
- 188 42. D. van der Meer, T. Kaufmann, A. A. Shadrin, C. Makowski, O. Frei, D. Roelfs, J. Monereo-
189 Sanchez, D. E. J. Linden, J. Rokicki, D. Alnaes, C. de Leeuw, W. K. Thompson, R. Loughnan,
190 C. C. Fan, L. T. Westlye, O. A. Andreassen, A. M. Dale, The genetic architecture of human
191 cortical folding. *Sci Adv* **7**, eabj9446 (2021).
- 192 43. S. Bahrami, K. Nordengen, A. A. Shadrin, O. Frei, D. van der Meer, A. M. Dale, L. T. Westlye,
193 O. A. Andreassen, T. Kaufmann, Distributed genetic architecture across the hippocampal
194 formation implies common neuropathology across brain disorders. *Nat Commun* **13**, 3436
195 (2022).
- 196 44. P. K. Albers, G. McVean, Dating genomic variants and shared ancestry in population-scale
197 sequencing data. *PLoS Biol* **18**, e3000586 (2020).
- 198 45. I. Libedinsky, Y. Wei, C. d. Leeuw, J. Rilling, D. Posthuma, M. P. v. d. Heuvel, Genetic timeline
199 of human brain and cognitive traits. *bioRxiv*, 2023.2002.2005.525539 (2023).
- 200 46. J. J. Hublin, A. Ben-Ncer, S. E. Bailey, S. E. Freidline, S. Neubauer, M. M. Skinner, I. Bergmann,
201 A. Le Cabec, S. Benazzi, K. Harvati, P. Gunz, New fossils from Jebel Irhoud, Morocco and the
202 pan-African origin of *Homo sapiens*. *Nature* **546**, 289-292 (2017).
- 203 47. D. Richter, R. Grun, R. Joannes-Boyau, T. E. Steele, F. Amani, M. Rue, P. Fernandes, J. P.
204 Raynal, D. Geraads, A. Ben-Ncer, J. J. Hublin, S. P. McPherron, The age of the hominin fossils
205 from Jebel Irhoud, Morocco, and the origins of the Middle Stone Age. *Nature* **546**, 293-296
206 (2017).
- 207 48. S. Davies, Behavioral Modernity in Retrospect. *Topoi* **40**, 221-232 (2021).
- 208 49. C. A. de Leeuw, J. M. Mooij, T. Heskes, D. Posthuma, MAGMA: generalized gene-set analysis
209 of GWAS data. *PLoS Comput Biol* **11**, e1004219 (2015).
- 210 50. Y. Wei, S. C. de Lange, L. H. Scholtens, K. Watanabe, D. J. Ardesch, P. R. Jansen, J. E. Savage,
211 L. Li, T. M. Preuss, J. K. Rilling, D. Posthuma, M. P. van den Heuvel, Genetic mapping and
212 evolutionary analysis of human-expanded cognitive networks. *Nat Commun* **10**, 4839 (2019).
- 213 51. H. Won, J. Huang, C. K. Opland, C. L. Hartl, D. H. Geschwind, Human evolved regulatory
214 elements modulate genes involved in cortical expansion and neurodevelopmental disease
215 susceptibility. *Nat Commun* **10**, 2396 (2019).
- 216 52. A. Liberzon, C. Birger, H. Thorvaldsdottir, M. Ghandi, J. P. Mesirov, P. Tamayo, The Molecular
217 Signatures Database (MSigDB) hallmark gene set collection. *Cell Syst* **1**, 417-425 (2015).
- 218 53. A. Subramanian, P. Tamayo, V. K. Mootha, S. Mukherjee, B. L. Ebert, M. A. Gillette, A.
219 Paulovich, S. L. Pomeroy, T. R. Golub, E. S. Lander, J. P. Mesirov, Gene set enrichment
220 analysis: a knowledge-based approach for interpreting genome-wide expression profiles. *Proc*
221 *Natl Acad Sci U S A* **102**, 15545-15550 (2005).
- 222 54. M. Kircher, D. M. Witten, P. Jain, B. J. O'Roak, G. M. Cooper, J. Shendure, A general framework
223 for estimating the relative pathogenicity of human genetic variants. *Nat Genet* **46**, 310-315
224 (2014).

- 225 55. O. A. Andreassen, W. K. Thompson, A. J. Schork, S. Ripke, M. Mattingsdal, J. R. Kelsoe, K. S.
226 Kendler, M. C. O'Donovan, D. Rujescu, T. Werge, P. Sklar, C. Psychiatric Genomics, D. Bipolar,
227 G. Schizophrenia Working, J. C. Roddey, C. H. Chen, L. McEvoy, R. S. Desikan, S. Djurovic, A.
228 M. Dale, Improved detection of common variants associated with schizophrenia and bipolar
229 disorder using pleiotropy-informed conditional false discovery rate. *PLoS Genet* **9**, e1003455
230 (2013).
- 231 56. M. Z. King, Zonglei; Ivry, Richard B.; Weiner, Kevin S., Transcriptomic Gradients Of The Human
232 Cerebellum.
- 233 57. X. Guell, J. D. E. Gabrieli, J. D. Schmahmann, Triple representation of language, working
234 memory, social and emotion processing in the cerebellum: convergent evidence from task and
235 seed-based resting-state fMRI analyses in a single large cohort. *Neuroimage* **172**, 437-449
236 (2018).
- 237 58. C. H. Chen, E. D. Gutierrez, W. Thompson, M. S. Panizzon, T. L. Jernigan, L. T. Eyler, C.
238 Fennema-Notestine, A. J. Jak, M. C. Neale, C. E. Franz, M. J. Lyons, M. D. Grant, B. Fischl, L.
239 J. Seidman, M. T. Tsuang, W. S. Kremen, A. M. Dale, Hierarchical genetic organization of human
240 cortical surface area. *Science* **335**, 1634-1636 (2012).
- 241 59. C. H. Chen, M. Fiecas, E. D. Gutierrez, M. S. Panizzon, L. T. Eyler, E. Vuoksima, W. K.
242 Thompson, C. Fennema-Notestine, D. J. Hagler, Jr., T. L. Jernigan, M. C. Neale, C. E. Franz,
243 M. J. Lyons, B. Fischl, M. T. Tsuang, A. M. Dale, W. S. Kremen, Genetic topography of brain
244 morphology. *Proc Natl Acad Sci U S A* **110**, 17089-17094 (2013).
- 245 60. C. Guissart, X. Latypova, P. Rollier, T. N. Khan, H. Stamberger, K. McWalter, M. T. Cho, S.
246 Kjaergaard, S. Weckhuysen, G. Lesca, T. Besnard, K. Ounap, L. Schema, A. G. Chiocchetti, M.
247 McDonald, J. de Bellescize, M. Vincent, H. Van Esch, S. Sattler, I. Forghani, I. Thiffault, C. M.
248 Freitag, D. S. Barbooth, M. Cadieux-Dion, R. Willaert, M. J. Guillen Sacoto, N. P. Safina, C.
249 Dubourg, L. Grote, W. Carre, C. Saunders, S. Pajusalu, E. Farrow, A. Boland, D. H. Karlowicz,
250 J. F. Deleuze, M. H. Wojcik, R. Pressman, B. Isidor, A. Vogels, W. Van Paesschen, L. Al-Gazali,
251 A. M. Al Shamsi, M. Claustres, A. Pujol, S. J. Sanders, F. Rivier, N. Leboucq, B. Cogne, S.
252 Sasorith, D. Sanlaville, K. Retterer, S. Odent, N. Katsanis, S. Bezieau, M. Koenig, E. E. Davis,
253 L. Pasquier, S. Kury, Dual Molecular Effects of Dominant RORA Mutations Cause Two Variants
254 of Syndromic Intellectual Disability with Either Autism or Cerebellar Ataxia. *Am J Hum Genet*
255 **102**, 744-759 (2018).
- 256 61. C. L. Chi, S. Martinez, W. Wurst, G. R. Martin, The isthmus organizer signal FGF8 is required for
257 cell survival in the prospective midbrain and cerebellum. *Development* **130**, 2633-2644 (2003).
- 258 62. S. Li, F. Qiu, A. Xu, S. M. Price, M. Xiang, Barhl1 regulates migration and survival of cerebellar
259 granule cells by controlling expression of the neurotrophin-3 gene. *J Neurosci* **24**, 3104-3114
260 (2004).
- 261 63. S. Valence, C. Garel, M. Barth, A. Toutain, C. Paris, D. Amsallem, M. A. Barthez, M. Mayer, D.
262 Rodriguez, L. Burglen, RELN and VLDLR mutations underlie two distinguishable clinico-
263 radiological phenotypes. *Clin Genet* **90**, 545-549 (2016).
- 264 64. M. Larouche, U. Beffert, J. Herz, R. Hawkes, The Reelin receptors Apoer2 and Vldlr coordinate
265 the patterning of Purkinje cell topography in the developing mouse cerebellum. *PLoS One* **3**,
266 e1653 (2008).
- 267 65. T. Wolfers, N. T. Doan, T. Kaufmann, D. Alnaes, T. Moberget, I. Agartz, J. K. Buitelaar, T.
268 Ueland, I. Melle, B. Franke, O. A. Andreassen, C. F. Beckmann, L. T. Westlye, A. F. Marquand,
269 Mapping the Heterogeneous Phenotype of Schizophrenia and Bipolar Disorder Using Normative
270 Models. *JAMA Psychiatry* **75**, 1146-1155 (2018).
- 271 66. T. Wolfers, J. Rokicki, D. Alnaes, P. Berthet, I. Agartz, S. M. Kia, T. Kaufmann, M. Zabihi, T.
272 Moberget, I. Melle, C. F. Beckmann, O. A. Andreassen, A. F. Marquand, L. T. Westlye,
273 Replicating extensive brain structural heterogeneity in individuals with schizophrenia and bipolar
274 disorder. *Hum Brain Mapp* **42**, 2546-2555 (2021).
- 275 67. N. C. Armstrong, R. C. Anderson, K. W. McDermott, Reelin: Diverse roles in central nervous
276 system development, health and disease. *Int J Biochem Cell Biol* **112**, 72-75 (2019).

- 277 68. M. Li, L. Huang, M. Grigoriou-Serbanescu, S. E. Bergen, M. Landen, C. M. Hultman, A. J.
278 Forstner, J. Strohmaier, J. Hecker, T. G. Schulze, B. Muller-Myhsok, A. Reif, P. B. Mitchell, N.
279 G. Martin, S. Cichon, M. M. Nothen, A. Alkelai, B. Lerer, S. Jamain, M. Leboyer, F. Bellivier, B.
280 Etain, J. P. Kahn, C. Henry, M. Rietschel, D. S. C. Moo, G. Swedish Bipolar Study, Convergent
281 Lines of Evidence Support LRP8 as a Susceptibility Gene for Psychosis. *Mol Neurobiol* **53**, 6608-
282 6619 (2016).
- 283 69. A. Okbay, Y. Wu, N. Wang, H. Jayashankar, M. Bennett, S. M. Nehzati, J. Sidorenko, H. Kweon,
284 G. Goldman, T. Gjorgjieva, Y. Jiang, B. Hicks, C. Tian, D. A. Hinds, R. Ahlskog, P. K. E.
285 Magnusson, S. Oskarsson, C. Hayward, A. Campbell, D. J. Porteous, J. Freese, P. Herd, T.
286 andMe Research, C. Social Science Genetic Association, C. Watson, J. Jala, D. Conley, P. D.
287 Koellinger, M. Johannesson, D. Laibson, M. N. Meyer, J. J. Lee, A. Kong, L. Yengo, D. Cesarini,
288 P. Turley, P. M. Visscher, J. P. Beauchamp, D. J. Benjamin, A. I. Young, Polygenic prediction of
289 educational attainment within and between families from genome-wide association analyses in
290 3 million individuals. *Nat Genet* **54**, 437-449 (2022).
- 291 70. Q. Wang, R. S. Dhindsa, K. Carss, A. R. Harper, A. Nag, I. Tachmazidou, D. Vitsios, S. V. V.
292 Deevi, A. Mackay, D. Muthas, M. Huhn, S. Monkley, H. Olsson, I. AstraZeneca Genomics, S.
293 Wasilewski, K. R. Smith, R. March, A. Platt, C. Haefliger, S. Petrovski, Rare variant contribution
294 to human disease in 281,104 UK Biobank exomes. *Nature* **597**, 527-532 (2021).
- 295 71. B. Fischl, D. H. Salat, E. Busa, M. Albert, M. Dieterich, C. Haselgrove, A. van der Kouwe, R.
296 Killiany, D. Kennedy, S. Klaveness, A. Montillo, N. Makris, B. Rosen, A. M. Dale, Whole brain
297 segmentation: automated labeling of neuroanatomical structures in the human brain. *Neuron* **33**,
298 341-355 (2002).
- 299 72. J. Diedrichsen, in *NeuroImage*. (2006), vol. 33, pp. 127-138.
- 300 73. C. Leys, C. Ley, O. Klein, P. Bernard, L. Licata, Detecting outliers: Do not use standard deviation
301 around the mean, use absolute deviation around the median. *Journal of Experimental Social*
302 *Psychology* **49**, 764-766 (2013).
- 303 74. L. W. de Jong, J. S. Vidal, L. E. Forsberg, A. P. Zijdenbos, T. Haight, I. Alzheimer's Disease
304 Neuroimaging, S. Sigurdsson, V. Gudnason, M. A. van Buchem, L. J. Launer, Allometric scaling
305 of brain regions to intra-cranial volume: An epidemiological MRI study. *Hum Brain Mapp* **38**, 151-
306 164 (2017).
- 307 75. C. Mankiw, M. T. M. Park, P. K. Reardon, A. M. Fish, L. S. Clasen, D. Greenstein, J. N. Giedd,
308 J. D. Blumenthal, J. P. Lerch, M. M. Chakravarty, A. Raznahan, Allometric Analysis Detects Brain
309 Size-Independent Effects of Sex and Sex Chromosome Complement on Human Cerebellar
310 Organization. *J Neurosci* **37**, 5221-5231 (2017).
- 311 76. K. J. Friston, *Statistical parametric mapping : the analysis of functional brain images*
312 (Elsevier/Academic Press, Amsterdam ; Boston, ed. 1st, 2007), pp. vii, 647 p.
- 313 77. R. Nassar, A. N. Kaczkurkin, C. H. Xia, A. Sotiras, M. Pehlivanova, T. M. Moore, A. Garcia de
314 La Garza, D. R. Roalf, A. F. G. Rosen, S. A. Lorch, K. Ruparel, R. T. Shinohara, C. Davatzikos,
315 R. C. Gur, R. E. Gur, T. D. Satterthwaite, Gestational Age is Dimensionally Associated with
316 Structural Brain Network Abnormalities Across Development. *Cereb Cortex* **29**, 2102-2114
317 (2019).
- 318 78. M. Pehlivanova, D. H. Wolf, A. Sotiras, A. N. Kaczkurkin, T. M. Moore, R. Ciric, P. A. Cook, A.
319 Garcia de La Garza, A. F. G. Rosen, K. Ruparel, A. Sharma, R. T. Shinohara, D. R. Roalf, R. C.
320 Gur, C. Davatzikos, R. E. Gur, J. W. Kable, T. D. Satterthwaite, Diminished Cortical Thickness
321 Is Associated with Impulsive Choice in Adolescence. *J Neurosci* **38**, 2471-2481 (2018).
- 322 79. H. W. Kuhn, The Hungarian method for the assignment problem. *Naval Research Logistics*
323 *Quarterly* **2**, 14 (1955).
- 324 80. J. M. Santos, M. Embrechts. (Springer Berlin Heidelberg, Berlin, Heidelberg, 2009), pp. 175-184.
- 325 81. T. M. Beasley, S. Erickson, D. B. Allison, Rank-based inverse normal transformations are
326 increasingly used, but are they merited? *Behav Genet* **39**, 580-595 (2009).
- 327 82. C. Bycroft, C. Freeman, D. Petkova, G. Band, L. T. Elliott, K. Sharp, A. Motyer, D. Vukcevic, O.
328 Delaneau, J. O'Connell, A. Cortes, S. Welsh, A. Young, M. Effingham, G. McVean, S. Leslie, N.

Allen, P. Donnelly, J. Marchini, The UK Biobank resource with deep phenotyping and genomic data. *Nature* **562**, 203-209 (2018).

83. A. P. Boyle, E. L. Hong, M. Hariharan, Y. Cheng, M. A. Schaub, M. Kasowski, K. J. Karczewski, J. Park, B. C. Hitz, S. Weng, J. M. Cherry, M. Snyder, Annotation of functional variation in personal genomes using RegulomeDB. *Genome Res* **22**, 1790-1797 (2012).
84. Z. Zhu, F. Zhang, H. Hu, A. Bakshi, M. R. Robinson, J. E. Powell, G. W. Montgomery, M. E. Goddard, N. R. Wray, P. M. Visscher, J. Yang, Integration of summary data from GWAS and eQTL studies predicts complex trait gene targets. *Nat Genet* **48**, 481-487 (2016).
85. A. Arnatkeviciute, B. D. Fulcher, A. Fornito, A practical guide to linking brain-wide gene expression and neuroimaging data. *Neuroimage* **189**, 353-367 (2019).
86. J. Quackenbush, Microarray data normalization and transformation. *Nat Genet* **32 Suppl**, 496-501 (2002).
87. M. Hawrylycz, J. A. Miller, V. Menon, D. Feng, T. Dolbeare, A. L. Guillozet-Bongaarts, A. G. Jegga, B. J. Aronow, C. K. Lee, A. Bernard, M. F. Glasser, D. L. Dierker, J. Menche, A. Szafer, F. Collman, P. Grange, K. A. Berman, S. Mihalas, Z. Yao, L. Stewart, A. L. Barabasi, J. Schulkin, J. Phillips, L. Ng, C. Dang, D. R. Haynor, A. Jones, D. C. Van Essen, C. Koch, E. Lein, Canonical genetic signatures of the adult human brain. *Nat Neurosci* **18**, 1832-1844 (2015).
88. B. D. Fulcher, M. A. Little, N. S. Jones, Highly comparative time-series analysis: the empirical structure of time series and their methods. *J R Soc Interface* **10**, 20130048 (2013).
89. C. Genomes Project, A. Auton, L. D. Brooks, R. M. Durbin, E. P. Garrison, H. M. Kang, J. O. Korbel, J. L. Marchini, S. McCarthy, G. A. McVean, G. R. Abecasis, A global reference for human genetic variation. *Nature* **526**, 68-74 (2015).
90. S. Mallick, H. Li, M. Lipson, I. Mathieson, M. Gymrek, F. Racimo, M. Zhao, N. Chennagiri, S. Nordenfelt, A. Tandon, P. Skoglund, I. Lazaridis, S. Sankararaman, Q. Fu, N. Rohland, G. Renaud, Y. Erlich, T. Willems, C. Gallo, J. P. Spence, Y. S. Song, G. Poletti, F. Balloux, G. van Driem, P. de Knijff, I. G. Romero, A. R. Jha, D. M. Behar, C. M. Bravi, C. Capelli, T. Hervig, A. Moreno-Estrada, O. L. Posukh, E. Balanovska, O. Balanovsky, S. Karachanak-Yankova, H. Sahakyan, D. Toncheva, L. Yepiskoposyan, C. Tyler-Smith, Y. Xue, M. S. Abdullah, A. Ruiz-Linares, C. M. Beall, A. Di Rienzo, C. Jeong, E. B. Starikovskaya, E. Metspalu, J. Parik, R. Villems, B. M. Henn, U. Hodoglugil, R. Mahley, A. Sajantila, G. Stamatoyannopoulos, J. T. Wee, R. Khusainova, E. Khusnutdinova, S. Litvinov, G. Ayodo, D. Comas, M. F. Hammer, T. Kivisild, W. Klitz, C. A. Winkler, D. Labuda, M. Bamshad, L. B. Jorde, S. A. Tishkoff, W. S. Watkins, M. Metspalu, S. Dryomov, R. Sukernik, L. Singh, K. Thangaraj, S. Paabo, J. Kelso, N. Patterson, D. Reich, The Simons Genome Diversity Project: 300 genomes from 142 diverse populations. *Nature* **538**, 201-206 (2016).
91. A. Federico, S. Monti, hypeR: an R package for geneset enrichment workflows. *Bioinformatics* **36**, 1307-1308 (2020).
92. A. D. Rouillard, G. W. Gunderesen, N. F. Fernandez, Z. Wang, C. D. Monteiro, M. G. McDermott, A. Ma'ayan, The harmonizome: a collection of processed datasets gathered to serve and mine knowledge about genes and proteins. *Database (Oxford)* **2016**, (2016).
93. R. N. Doan, B. I. Bae, B. Cubelos, C. Chang, A. A. Hossain, S. Al-Saad, N. M. Mukaddes, O. Oner, M. Al-Saffar, S. Balkhy, G. G. Gascon, A. Homozygosity Mapping Consortium for, M. Nieto, C. A. Walsh, Mutations in Human Accelerated Regions Disrupt Cognition and Social Behavior. *Cell* **167**, 341-354 e312 (2016).
94. D. Demontis, R. K. Walters, J. Martin, M. Mattheisen, T. D. Als, E. Agerbo, G. Baldursson, R. Belliveau, J. Bybjerg-Grauholm, M. Baekvad-Hansen, F. Cerrato, K. Chambert, C. Churchhouse, A. Dumont, N. Eriksson, M. Gandal, J. I. Goldstein, K. L. Grasby, J. Grove, O. O. Gudmundsson, C. S. Hansen, M. E. Hauberg, M. V. Hollegaard, D. P. Howrigan, H. Huang, J. B. Maller, A. R. Martin, N. G. Martin, J. Moran, J. Pallesen, D. S. Palmer, C. B. Pedersen, M. G. Pedersen, T. Poterba, J. B. Poulsen, S. Ripke, E. B. Robinson, F. K. Satterstrom, H. Stefansson, C. Stevens, P. Turley, G. B. Walters, H. Won, M. J. Wright, A. W. G. o. t. P. G. Consortium, L. Early, C. Genetic Epidemiology, T. andMe Research, O. A. Andreassen, P. Asherson, C. L. Burton, D. I. Boomsma, B. Cormand, S. Dalsgaard, B. Franke, J. Gelernter, D. Geschwind, H. Hakonarson,

382 J. Haavik, H. R. Kranzler, J. Kuntsi, K. Langley, K. P. Lesch, C. Middeldorp, A. Reif, L. A. Rohde,
383 P. Roussos, R. Schachar, P. Sklar, E. J. S. Sonuga-Barke, P. F. Sullivan, A. Thapar, J. Y. Tung,
384 I. D. Waldman, S. E. Medland, K. Stefansson, M. Nordentoft, D. M. Hougaard, T. Werge, O.
385 Mors, P. B. Mortensen, M. J. Daly, S. V. Faraone, A. D. Borglum, B. M. Neale, Discovery of the
386 first genome-wide significant risk loci for attention deficit/hyperactivity disorder. *Nat Genet* **51**,
387 63-75 (2019).

388 95. J. Grove, S. Ripke, T. D. Als, M. Mattheisen, R. K. Walters, H. Won, J. Pallesen, E. Agerbo, O.
389 A. Andreassen, R. Anney, S. Awashti, R. Belliveau, F. Bettella, J. D. Buxbaum, J. Bybjerg-
390 Grauholm, M. Baekvad-Hansen, F. Cerrato, K. Chambert, J. H. Christensen, C. Churchhouse,
391 K. Dellenvall, D. Demontis, S. De Rubeis, B. Devlin, S. Djurovic, A. L. Dumont, J. I. Goldstein,
392 C. S. Hansen, M. E. Hauberg, M. V. Hollegaard, S. Hope, D. P. Howrigan, H. Huang, C. M.
393 Hultman, L. Klei, J. Maller, J. Martin, A. R. Martin, J. L. Moran, M. Nyegaard, T. Naerland, D. S.
394 Palmer, A. Palotie, C. B. Pedersen, M. G. Pedersen, T. dPoterba, J. B. Poulsen, B. S. Pourcain,
395 P. Qvist, K. Rehnstrom, A. Reichenberg, J. Reichert, E. B. Robinson, K. Roeder, P. Roussos, E.
396 Saemundsen, S. Sandin, F. K. Satterstrom, G. Davey Smith, H. Stefansson, S. Steinberg, C. R.
397 Stevens, P. F. Sullivan, P. Turley, G. B. Walters, X. Xu, C. Autism Spectrum Disorder Working
398 Group of the Psychiatric Genomics, Bupgen, C. Major Depressive Disorder Working Group of
399 the Psychiatric Genomics, T. andMe Research, K. Stefansson, D. H. Geschwind, M. Nordentoft,
400 D. M. Hougaard, T. Werge, O. Mors, P. B. Mortensen, B. M. Neale, M. J. Daly, A. D. Borglum,
401 Identification of common genetic risk variants for autism spectrum disorder. *Nat Genet* **51**, 431-
402 444 (2019).

403 96. N. Mullins, A. J. Forstner, K. S. O'Connell, B. Coombes, J. R. I. Coleman, Z. Qiao, T. D. Als, T.
404 B. Bigdeli, S. Borte, J. Bryois, A. W. Charney, O. K. Drange, M. J. Gandal, S. P. Hagenaars, M.
405 Ikeda, N. Kamitaki, M. Kim, K. Krebs, G. Panagiotaropoulou, B. M. Schilder, L. G. Sloofman, S.
406 Steinberg, V. Trubetskoy, B. S. Winsvold, H. H. Won, L. Abramova, K. Adorjan, E. Agerbo, M.
407 Al Eissa, D. Albani, N. Alliey-Rodriguez, A. Anjorin, V. Antilla, A. Antoniou, S. Awasthi, J. H.
408 Baek, M. Baekvad-Hansen, N. Bass, M. Bauer, E. C. Beins, S. E. Bergen, A. Birner, C. Bocker
409 Pedersen, E. Boen, M. P. Boks, R. Bosch, M. Brum, B. M. Brumpton, N. Brunkhorst-Kanaan, M.
410 Budde, J. Bybjerg-Grauholm, W. Byerley, M. Cairns, M. Casas, P. Cervantes, T. K. Clarke, C.
411 Cruceanu, A. Cuellar-Barboza, J. Cunningham, D. Curtis, P. M. Czerski, A. M. Dale, N. Dalkner,
412 F. S. David, F. Degenhardt, S. Djurovic, A. L. Dobbyn, A. Douzenis, T. Elvsashagen, V. Escott-
413 Price, I. N. Ferrier, A. Fiorentino, T. M. Foroud, L. Forty, J. Frank, O. Frei, N. B. Freimer, L.
414 Frisen, K. Gade, J. Garnham, J. Gelernter, M. Giortz Pedersen, I. R. Gizer, S. D. Gordon, K.
415 Gordon-Smith, T. A. Greenwood, J. Grove, J. Guzman-Parra, K. Ha, M. Haraldsson, M.
416 Hautzinger, U. Heilbronner, D. Hellgren, S. Herms, P. Hoffmann, P. A. Holmans, L. Huckins, S.
417 Jamain, J. S. Johnson, J. L. Kalman, Y. Kamatani, J. L. Kennedy, S. Kittel-Schneider, J. A.
418 Knowles, M. Kogevinas, M. Koromina, T. M. Kranz, H. R. Kranzler, M. Kubo, R. Kupka, S. A.
419 Kushner, C. Lavebratt, J. Lawrence, M. Leber, H. J. Lee, P. H. Lee, S. E. Levy, C. Lewis, C.
420 Liao, S. Lucae, M. Lundberg, D. J. MacIntyre, S. H. Magnusson, W. Maier, A. Maihofer, D.
421 Malaspina, E. Maratou, L. Martinsson, M. Mattheisen, S. A. McCarroll, N. W. McGregor, P.
422 McGuffin, J. D. McKay, H. Medeiros, S. E. Medland, V. Millischer, G. W. Montgomery, J. L.
423 Moran, D. W. Morris, T. W. Muhleisen, N. O'Brien, C. O'Donovan, L. M. Olde Loohuis, L. Oruc,
424 S. Papiol, A. F. Pardini, A. Perry, A. Pfennig, E. Porichi, J. B. Potash, D. Quested, T. Raj, M.
425 H. Rapaport, J. R. DePaulo, E. J. Regeer, J. P. Rice, F. Rivas, M. Rivera, J. Roth, P. Roussos,
426 D. M. Ruderfer, C. Sanchez-Mora, E. C. Schulte, F. Senner, S. Sharp, P. D. Shilling, E.
427 Sigurdsson, L. Sirignano, C. Slaney, O. B. Smeland, D. J. Smith, J. L. Sobell, C. Soholm Hansen,
428 M. Soler Artigas, A. T. Spijker, D. J. Stein, J. S. Strauss, B. Swiatkowska, C. Terao, T. E.
429 Thorgeirsson, C. Toma, P. Tooney, E. E. Tsermpini, M. P. Vawter, H. Vedder, J. T. R. Walters,
430 S. H. Witt, S. Xi, W. Xu, J. M. K. Yang, A. H. Young, H. Young, P. P. Zandi, H. Zhou, L. Zillich,
431 H. A.-I. Psychiatry, R. Adolfsson, I. Agartz, M. Alda, L. Alfredsson, G. Babadjanova, L. Backlund,
432 B. T. Baune, F. Bellivier, S. Bengesser, W. H. Berrettini, D. H. R. Blackwood, M. Boehnke, A. D.
433 Borglum, G. Breen, V. J. Carr, S. Catts, A. Corvin, N. Craddock, U. Dannlowski, D. Dikeos, T.
434 Esko, B. Etain, P. Ferentinos, M. Frye, J. M. Fullerton, M. Gawlik, E. S. Gershon, F. S. Goes, M.

435 J. Green, M. Grigoriu-Serbanescu, J. Hauser, F. Henskens, J. Hillert, K. S. Hong, D. M.
436 Hougaard, C. M. Hultman, K. Hveem, N. Iwata, A. V. Jablensky, I. Jones, L. A. Jones, R. S.
437 Kahn, J. R. Kelsoe, G. Kirov, M. Landen, M. Leboyer, C. M. Lewis, Q. S. Li, J. Lissowska, C.
438 Lochner, C. Loughland, N. G. Martin, C. A. Mathews, F. Mayoral, S. L. McElroy, A. M. McIntosh,
439 F. J. McMahon, I. Melle, P. Michie, L. Milani, P. B. Mitchell, G. Morken, O. Mors, P. B. Mortensen,
440 B. Mowry, B. Muller-Myhsok, R. M. Myers, B. M. Neale, C. M. Nievergelt, M. Nordentoft, M. M.
441 Nothen, M. C. O'Donovan, K. J. Oedegaard, T. Olsson, M. J. Owen, S. A. Paciga, C. Pantelis,
442 C. Pato, M. T. Pato, G. P. Patrinos, R. H. Perlis, D. Posthuma, J. A. Ramos-Quiroga, A. Reif, E.
443 Z. Reininghaus, M. Ribases, M. Rietschel, S. Ripke, G. A. Rouleau, T. Saito, U. Schall, M.
444 Schalling, P. R. Schofield, T. G. Schulze, L. J. Scott, R. J. Scott, A. Serretti, C. Shannon
445 Weickert, J. W. Smoller, H. Stefansson, K. Stefansson, E. Stordal, F. Streit, P. F. Sullivan, G.
446 Turecki, A. E. Vaaler, E. Vieta, J. B. Vincent, I. D. Waldman, T. W. Weickert, T. Werge, N. R.
447 Wray, J. A. Zwart, J. M. Biernacka, J. I. Nurnberger, S. Cichon, H. J. Edenberg, E. A. Stahl, A.
448 McQuillin, A. Di Florio, R. A. Ophoff, O. A. Andreassen, Genome-wide association study of more
449 than 40,000 bipolar disorder cases provides new insights into the underlying biology. *Nat Genet*
450 **53**, 817-829 (2021).

97. N. R. Wray, S. Ripke, M. Mattheisen, M. Trzaskowski, E. M. Byrne, A. Abdellaoui, M. J. Adams,
451 E. Agerbo, T. M. Air, T. M. F. Andlauer, S. A. Bacanu, M. Baekvad-Hansen, A. F. T. Beekman,
452 T. B. Bigdeli, E. B. Binder, D. R. H. Blackwood, J. Bryois, H. N. Buttenschon, J. Bybjerg-
453 Grauholm, N. Cai, E. Castelao, J. H. Christensen, T. K. Clarke, J. I. R. Coleman, L. Colodro-
454 Conde, B. Couvy-Duchesne, N. Craddock, G. E. Crawford, C. A. Crowley, H. S. Dashti, G.
455 Davies, I. J. Deary, F. Degenhardt, E. M. Derks, N. Direk, C. V. Dolan, E. C. Dunn, T. C. Eley,
456 N. Eriksson, V. Escott-Price, F. H. F. Kiadeh, H. K. Finucane, A. J. Forstner, J. Frank, H. A.
457 Gaspar, M. Gill, P. Giusti-Rodriguez, F. S. Goes, S. D. Gordon, J. Grove, L. S. Hall, E. Hannon,
458 C. S. Hansen, T. F. Hansen, S. Herms, I. B. Hickie, P. Hoffmann, G. Homuth, C. Horn, J. J.
459 Hottenga, D. M. Hougaard, M. Hu, C. L. Hyde, M. Ising, R. Jansen, F. Jin, E. Jorgenson, J. A.
460 Knowles, I. S. Kohane, J. Kraft, W. W. Kretschmar, J. Krogh, Z. Kutalik, J. M. Lane, Y. Li, Y. Li,
461 P. A. Lind, X. Liu, L. Lu, D. J. MacIntyre, D. F. MacKinnon, R. M. Maier, W. Maier, J. Marchini,
462 H. Mbarek, P. McGrath, P. McGuffin, S. E. Medland, D. Mehta, C. M. Middeldorp, E. Mihailov,
463 Y. Milanese, L. Milani, J. Mill, F. M. Mondimore, G. W. Montgomery, S. Mostafavi, N. Mullins,
464 M. Nauck, B. Ng, M. G. Nivard, D. R. Nyholt, P. F. O'Reilly, H. Oskarsson, M. J. Owen, J. N.
465 Painter, C. B. Pedersen, M. G. Pedersen, R. E. Peterson, E. Pettersson, W. J. Peyrot, G. Pistis,
466 D. Posthuma, S. M. Purcell, J. A. Quiroz, P. Qvist, J. P. Rice, B. P. Riley, M. Rivera, S. Saeed
467 Mirza, R. Saxena, R. Schoevers, E. C. Schulte, L. Shen, J. Shi, S. I. Shyn, E. Sigurdsson, G. B.
468 C. Sinnamon, J. H. Smit, D. J. Smith, H. Stefansson, S. Steinberg, C. A. Stockmeier, F. Streit,
469 J. Strohmaier, K. E. Tansey, H. Teismann, A. Teumer, W. Thompson, P. A. Thomson, T. E.
470 Thorgeirsson, C. Tian, M. Traylor, J. Treutlein, V. Trubetsky, A. G. Uitterlinden, D. Umbricht, S.
471 Van der Auwera, A. M. van Hemert, A. Viktorin, P. M. Visscher, Y. Wang, B. T. Webb, S. M.
472 Weinsheimer, J. Wellmann, G. Willemsen, S. H. Witt, Y. Wu, H. S. Xi, J. Yang, F. Zhang, eQTLgen,
473 andMe, V. Arolt, B. T. Baune, K. Berger, D. I. Boomsma, S. Cichon, U. Dannlowski, E. C. J. de
474 Geus, J. R. DePaulo, E. Domenici, K. Domschke, T. Esko, H. J. Grabe, S. P. Hamilton, C.
475 Hayward, A. C. Heath, D. A. Hinds, K. S. Kendler, S. Kloiber, G. Lewis, Q. S. Li, S. Lucae, P. F.
476 A. Madden, P. K. Magnusson, N. G. Martin, A. M. McIntosh, A. Metspalu, O. Mors, P. B.
477 Mortensen, B. Muller-Myhsok, M. Nordentoft, M. M. Nothen, M. C. O'Donovan, S. A. Paciga, N.
478 L. Pedersen, B. Penninx, R. H. Perlis, D. J. Porteous, J. B. Potash, M. Preisig, M. Rietschel, C.
479 Schaefer, T. G. Schulze, J. W. Smoller, K. Stefansson, H. Tiemeier, R. Uher, H. Volzke, M. M.
480 Weissman, T. Werge, A. R. Winslow, C. M. Lewis, D. F. Levinson, G. Breen, A. D. Borglum, P.
481 F. Sullivan, C. Major Depressive Disorder Working Group of the Psychiatric Genomics, Genome-
482 wide association analyses identify 44 risk variants and refine the genetic architecture of major
483 depression. *Nat Genet* **50**, 668-681 (2018).
98. A. F. Pardinas, P. Holmans, A. J. Pocklington, V. Escott-Price, S. Ripke, N. Carrera, S. E. Legge,
484 S. Bishop, D. Cameron, M. L. Hamshere, J. Han, L. Hubbard, A. Lynham, K. Mantripragada, E.
485 Rees, J. H. MacCabe, S. A. McCarroll, B. T. Baune, G. Breen, E. M. Byrne, U. Dannlowski, T.

488 C. Eley, C. Hayward, N. G. Martin, A. M. McIntosh, R. Plomin, D. J. Porteous, N. R. Wray, A.
489 Caballero, D. H. Geschwind, L. M. Huckins, D. M. Ruderfer, E. Santiago, P. Sklar, E. A. Stahl,
490 H. Won, E. Agerbo, T. D. Als, O. A. Andreassen, M. Baekvad-Hansen, P. B. Mortensen, C. B.
491 Pedersen, A. D. Borglum, J. Bybjerg-Grauholm, S. Djurovic, N. Durmishi, M. G. Pedersen, V.
492 Golimbet, J. Grove, D. M. Hougaard, M. Mattheisen, E. Molden, O. Mors, M. Nordentoft, M.
493 Pejovic-Milovancevic, E. Sigurdsson, T. Silagadze, C. S. Hansen, K. Stefansson, H. Stefansson,
494 S. Steinberg, S. Tosato, T. Werge, G. Consortium, C. Consortium, D. A. Collier, D. Rujescu, G.
495 Kirov, M. J. Owen, M. C. O'Donovan, J. T. R. Walters, Common schizophrenia alleles are
496 enriched in mutation-intolerant genes and in regions under strong background selection. *Nat*
497 *Genet* **50**, 381-389 (2018).

498 99. O. A. Andreassen, S. Djurovic, W. K. Thompson, A. J. Schork, K. S. Kendler, M. C. O'Donovan,
499 D. Rujescu, T. Werge, M. van de Bunt, A. P. Morris, M. I. McCarthy, G. International Consortium
500 for Blood Pressure, R. Diabetes Genetics, C. Meta-analysis, G. Psychiatric Genomics
501 Consortium Schizophrenia Working, J. C. Roddey, L. K. McEvoy, R. S. Desikan, A. M. Dale,
502 Improved detection of common variants associated with schizophrenia by leveraging pleiotropy
503 with cardiovascular-disease risk factors. *Am J Hum Genet* **92**, 197-209 (2013).

504 100. O. B. Smeland, O. Frei, A. Shadrin, K. O'Connell, C. C. Fan, S. Bahrami, D. Holland, S. Djurovic,
505 W. K. Thompson, A. M. Dale, O. A. Andreassen, Discovery of shared genomic loci using the
506 conditional false discovery rate approach. *Hum Genet* **139**, 85-94 (2020).

509 Acknowledgements

510
511 This work was performed on the Tjeneste for Sensitive Data (TSD) facilities, owned by the University of
512 Oslo, operated and developed by the TSD service group at the University of Oslo, IT-Department (USIT)
513 and on resources provided by UNINETT Sigma2—the National Infrastructure for High Performance
514 Computing and Data Storage in Norway. The research has been conducted using the UK Biobank
515 Resource (access code 27412) and using summary statistics for various brain disorders. We would like
516 to thank the research participants and employees of UK Biobank and the consortia contributing
517 summary statistics for making this work possible.

518
519 **Funding:** The authors were funded by the South-Eastern Norway Regional Health Authority (TM: 2021-
520 040; OAA: 2013-123, 2017-112, 2019-108. LTW: 2014-097, 2015-073, 2016-083), the Research
521 Council of Norway (TK: 276082, 323961. OAA: 213837, 223273, 248778, 273291, 262656, 229129,
522 283798, 311993. LTW: 204966, 249795, 273345), Norwegian Health Association (SB: 22731), Stiftelsen
523 Kristian Gerhard Jebsen, and the European Research Council (LTW: ERCStG 802998). The funding
524 bodies had no role in the analysis or interpretation of the data; the preparation, review or approval of
525 the manuscript; nor in the decision to submit the manuscript for publication.

526
527 **Author contributions:** TM originally conceived of the project. TM, DvdM and SB performed the
528 analyses. TM, LTW and OAA wrote the initial draft of the manuscript. All authors discussed the results
529 and contributed to the final manuscript.

530

531 **Competing interests:** O.A.A. has received speaker's honorarium from Lundbeck and is a consultant to
532 HealthLytix. A.M.D. is the founder of and holds equity in CorTechs Labs Inc. and serves on its Scientific
533 Advisory Board. A.M.D. is also a member of the Scientific Advisory Board of Human Longevity Inc. and
534 receives funding through research agreements with General Electric Healthcare and Medtronic Inc. The
535 terms of these arrangements have been reviewed and approved by UCSD in accordance with its
536 conflict-of-interest policies. A.M.D. is an inventor on a patent related to this work, filed by CorTechs Labs
537 Inc. (9 US-7324842B2, filed 22 January 2002, published 29-01-2008). The other authors declare that
538 they have no competing interests.

539

540 **Data availability**

541 In this study we used brain imaging and genetics data from the UK Biobank
542 [<https://www.ukbiobank.ac.uk/>], and GWAS summary statistics obtained from the Psychiatric Genomics
543 Consortium [<https://www.med.unc.edu/pgc/shared-methods/>] and GWAS catalog
544 [<https://www.ebi.ac.uk/gwas/>]. The summary statistics for cerebellar morphology derived in this study
545 are available in our github repository [<https://github.com/norment/open-science>] (*will make this public upon acceptance*). FUMA results are available online (*will make this public upon acceptance*). The
546 Human Genome Dating Dataset (HGD) is available at <https://human.genome.dating>.

548

549 **Code availability**

550 All code and software needed to generate the results is available as part of public resources, specifically
551 FreeSurfer (<https://surfer.nmr.mgh.harvard.edu>), SUIT (<https://github.com/jdiedrichsen/suit>), OPNMF
552 (<https://github.com/asotiras/brainparts>), MOSTest (<https://github.com/precimed/mostest>), FUMA
553 (<https://fuma.ctglab.nl/>), MAGMA (<https://ctg.cncr.nl/software/magma>), abagen
554 (<https://github.com/rmarkello/abagen>), conjunctural FDR (<https://github.com/precimed/pleiofdr/>) and
555 LD score regression (<https://github.com/bulik/ldsc>).

556

557 **Supplementary Materials:**

- 558 1. Supplementary Figures
- 559 2. Supplementary Information – Data Tables 1-36